Review of Polar Stratospheric Cloud Microphysics and Chemistry

Douglas Lowe

The University of Manchester

A. Robert MacKenzie

Lancaster University

Abstract

The solid and liquid particles which constitute polar stratospheric clouds (PSCs) are of manifold importance to the meteorology of the stratosphere. The heterogeneous reactions which take place on and within these particles release halogens from relatively inert reservoir species into forms which can destroy ozone in the polar spring. In addition, solid PSC particles are instrumental in the physical removal of nitrogen oxides (denitrification) and water (dehydration) of regions of the polar stratosphere. Denitrification, in particular, allows extended ozone destruction by slowing the conversion of chlorine radicals back into reservoir species.

We review the historical development of PSC studies, with particular emphasis on results from the last decade, encompassing developments in observations, in laboratory experiments, and in theoretical treatments. The technical challenge of measuring sufficient of the parameters describing any given polar stratospheric cloud, to allow its microphysics to be understood, has driven forward balloon-borne, aircraft, and satellite instrumentation. The technical challenge of finding suitable laboratory

proxies for PSCs, in order to observe the microphysics under controlled conditions, has resulted in a wide variety of experimental designs, some of which maximise the probability of observing phase change, others of which mimic the surface-volume ratios of PSCs more closely. The challenge to theory presented by PSCs has resulted in improvements in the thermodynamics of concentrated inorganic solutions of volatile compounds, and a new general theory of freezing of water ice from concentrated aqueous solutions. Of the major processes involving PSCs, heterogeneous reaction probabilities for ternary $HNO_3/H_2SO_4/H_2O$ solutions, and heterogeneous freezing to produce nitric acid hydrates, are the least well understood.

Key words: Polar stratospheric cloud; stratospheric ozone depletion; stratospheric aerosol; denitrification; heterogeneous chemistry; freezing nucleation

---

1 Historical overview

The first polar stratospheric clouds (PSCs) observed were the beautiful nacreous, or mother-of-pearl, clouds which are quite commonly visible above the mountains of Scandinavia and the Antarctic peninsula, but are also occasionally seen in the middle latitudes (Stanford and Davis, 1974, simply type "nacreous cloud" into an internet search engine for recent images). For example, as pointed out to us by an anonymous reviewer, PSCs were recorded in 1901 by the Danish painter Jorgensen. By the mid-20th century, scientists had found that the clouds formed at altitudes of around 25 km (i.e., the lower stratosphere) and temperatures near -80 ℃. Mother-of-pearl clouds are water ice clouds, formed within stratospheric gravity waves. Their rich colouration is the result of forward diffraction of sunlight by the particles; the changes in colour occur because of the variations in particle size along the profile of the wave (e.g., see Tolbert and Toon, 2001, and references within).

From satellite and other observations in the last quarter of the twentieth century, a simple three-stage model of PSC development began to emerge (Figure 1). This model starts with the background aerosol particles — consisting of supercooled sulphuric acid solution with about 75% by weight H_2SO_4 (Rosen, 1971) — which form the stratospheric Junge layer. As the temperature decreases these particles may freeze to form sulphuric acid tetrahydrate (SAT) (e.g., see Dye et al., 1992, and references within), although this step was not always included (e.g. Drdla and Turco, 1991). The essential features of this theory were that nucleation of NAT onto the background sulphate particles would occur below the NAT equilibrium temperature ($192 < T_{NAT} < 197\,\mathrm{K}$, for typical partial pressures of water vapour and nitric acid in the lower stratosphere), leading to Type I PSCs, and further cooling to below the ice frost point ($188 < T_{ICE} < 190\,\mathrm{K}$) would result in the nucleation of water ice onto the NAT particles to form Type II PSCs.

However observational data suggested that the formation of PSCs was more complicated. Measurements in the presence of Type I PSCs found that substantial transfer of HNO_3 from the vapour to condensed phase only occurred about 3–4 K below T_{NAT}, and that the HNO_3 partial pressures were significantly higher than NAT vapour pressures (Rosen et al., 1989; Hofmann et al., 1990; Schlager et al., 1990). These observations suggested that some unidentified process was causing a hysteresis effect, where the formation of NAT was hampered until 3–4 K below T_{NAT}, but, once formed, it could exist up to T_{NAT}. This led to proposals for different requirements for the formation of NAT particles, ranging from the necessity of SAT as a nucleus, to free energy barriers (see Dye et al., 1992, and references within). Rosen et al. (1989) interpreted the difference in vapour pressures as indicating the presence of another meta-

stable nitric acid particle, possibly an amorphous solid-solution with variable composition (Hamill et al., 1988). Analysis of lidar measurements (Browell et al., 1990; Toon et al., 1990) identified two distinct subtypes of nitric acid particles. Non-spherical particles, with a spherical volume-equivalent-radius exceeding 1.0 μm were denoted as Type Ia, while Type Ib particles were classified as spherical with radii near 0.5 μm.

Hanson (1990) suggested that, when the gas phase has not reached equilibrium with NAT, supercooled nitric acid solutions could condense up to a few degrees above the frost point. Laboratory experiments on the uptake of HNO_3 by H_2SO_4/H_2O solutions led Zhang et al. (1993) and Molina et al. (1993) to conclude that, below T_{NAT}, the background sulphuric droplets would take up H_2O and HNO_3 to form a supercooled ternary solution (STS) particle, composed of $HNO_3/H_2SO_4/H_2O$, which would freeze to NAT. PSC theory was, therefore, shifting away from the simple three-stage model focused on the solid NAT and ice particles, with other particle phases merely facilitating phase-changes. Thermodynamical modelling studies by Carslaw et al. (1994) and Tabazadeh et al. (1994) demonstrated that STS particles could have HNO_3 mass fractions as high as 41%, with H_2SO_4 as low as 3%, in stratospheric conditions, provided the particles do not freeze. Tabazadeh et al. (1994) showed that the increase in mass of the particles — due to the uptake of H_2O and HNO_3 — was sufficient to fulfill the size and shape definitions given for Type Ib particles by Toon et al. (1990). Carslaw et al. (1994) compared particle volumes observed by Dye et al. (1992) with those predicted using the different proposed PSC phases (Figure 2) and demonstrated that PSCs composed of STS particles fitted the data much better than those composed of NAT particles. Bulk freezing experiments (Koop et al., 1995) and theoretical stud-

ies (MacKenzie et al., 1995) suggested that homogeneous nucleation rates of NAT from STS were low enough to allow the existence of these liquid particles below T_{NAT} without freezing.

The model of PSC development was now a lot more complicated (Figure 3, and Peter (1997)). Three major types of PSC particle had been identified: water ice, NAT and STS. However it was not until five years later that in-situ measurements of particle compositions in the Arctic positively identified the existence of NAT (Voigt et al., 2000a) and STS (Voigt et al., 2000b) in the stratosphere. As the temperature decreases, the background sulphuric acid aerosol particles remain liquid, taking up H_2O and HNO_3 from the gas phase to become STS particles a few degrees below T_{NAT}. However the principal nucleation mechanisms in the stratosphere for converting these liquid particles to solid ice and NAT particles are still not clear.

Below, we divide our review of PSC studies into three broad sections: a discussion of the instrumentation deployed in fieldwork, a discussion of PSC composition in detail, and a discussion of the effects of PSCs.

2 Fieldwork Instrumentation

The data used for PSC studies ranges from retrieved atmospheric composition over synoptic scales by satellite-mounted instruments, to the in-situ measurement of particle compositions and gas-phase mixing ratios by balloon and aircraft mounted instruments. Most aspects of the stratosphere, from air temperature and the mixing ratios of individual components, to the size, number and composition of aerosol particles, can be studied. However, it is not al-

ways possible to measure all the atmospheric aspects relevant to a a PSC simultaneously and with the required precision.

2.1 Measuring Aerosol Properties

Even for a homogeneously mixed air parcel, an aerosol population will vary across several different properties, i.e., variations that produce the number, surface area, and volume density distributions, as well as variations in shape, composition and phase (e.g., Jaenicke, 1998; Seinfeld and Pandis, 2006). Each of these characteristics can be represented in a number of different ways, the accuracies of which are usually determined by the limitations of the instruments being used. There are few instruments which can measure more than a one or two of these characteristics, and none which will measure all of them (Hinds, 1999; Vincent, 2007).

The information content of data from an aerosol instrument is limited by the number of different measurements the instrument makes of the aerosol. For example, a single wavelength lidar will measure the backscatter and depolarisation caused by an aerosol. From these, and by making some assumptions, we can derive the total aerosol volume concentration (μm^3 m^{-3}), and an indication of the average particle shape. The total aerosol volume concentration is determined by the number density and size distribution of the aerosol so, by assuming a standard value for one of these characteristics, we can obtain an estimate of the other.

To minimise the assumptions required to characterise the aerosol, a number of different instruments, chosen to complement each other, can be used. For

instance, it is becoming more common to use data from both optical particle counters and mass spectrometers to obtain data on both the sizes, number, and compositions of the particles (Peter, 1996; Schreiner et al., 1999). However, care must be taken that such combinations are viable. The data collected by instruments provide a snap-shot of the atmospheric conditions. We must make sure that the samples, from which the data are obtained, are related both temporally and spatially, otherwise the information is likely to be misleading when combined.

2.2 Synoptic and Global-Scale Measurements

The first measurements of sub-visible PSCs were made using the SAM-II instrument, mounted on the Nimbus-7 satellite (McCormick et al., 1981, 1982). SAM-II, and the instruments which followed, are solar occultation photometers that measure the attenuation of light from the Sun as it passes through the atmosphere. Lines of sight through the atmosphere to the Sun are only possible during sunrise and sunset, and measurements have sample volumes of several hundred cubic kilometres. Analysis of each measurement is focused on an air parcel centred at the point along the line of sight between the satellite and the Sun which is closest to the surface of the Earth (SAGE III ATBD Team, 2002, available from NASA Langley Research Centre at http://www-sage3.larc.nasa.gov/).

The data are processed to obtain the contributions to the solar attenuation of effects such as Rayleigh scattering, aerosol extinction and absorption by gaseous species. To produce vertical profiles, the contributions of the higher altitudes to each measurement are subtracted. SAM-II measured only the 1 μm

wavelength; however modern instruments take measurements across a number of different wavelengths — the Stratospheric Aerosol and Gas Experiment (SAGE) III instrument produces data over 8 wavelengths between 0.29 and 1.55 μm (SAGE III ATBD Team, 2002), while the Polar Ozone and Aerosol Measurement (POAM) III instrument produces aerosol extinction data for 6 wavelengths between 0.353 and 1.018 μm (Strawa et al., 2002).

Following McCormick et al. (1981), Poole and Pitts (1994) used the SAM-II aerosol extinction profiles to develop a long term PSC climatology. This in turn has been extended and improved by Fromm et al. (2003) to become a unified stratospheric aerosol and cloud database which combines data from the SAM II, SAGE II, and POAM II/III missions. By taking the ratio of the aerosol extinctions at 0.603 μm and 1.018 μm, Strawa et al. (2002) have demonstrated that POAM-III data can be used to distinguish synoptic-scale PSCs of types Ia and Ib (Figure 4). They validated their method using lidar observations that were coincident with POAM observations. Poole et al. (2003), Lee et al. (2003) and Kim et al. (2006) have extended the use of this technique to the analysis of SAGE III measurements and ILAS-I/ILAS-II measurements, respectively. Relative extinction coefficients are calculated using adjacent transmittance profiles, one containing a PSC signature, the second containing none. A non-linear least squares fit method was used to compare the measured extinction spectra with spectra derived using Mie-scattering theory for single (Lee et al., 2003) and dual (Kim et al., 2006) phase PSCs. Using this method they were able to determine, within uncertainties of 25–40%, PSC compositions and effective particle radii.

Other limb-sounding instruments, mounted on balloons and satellites, have been also been used to detect PSCs. These instruments scan the atmosphere

above the horizon in a similar manner to solar occultation photometers, but are not orientated towards the Sun. Instead they measure the scattering of upwelling tropospheric radiation into the limb view, or the thermal infrared emission from the troposphere, stratosphere and mesosphere. These methods are particularly well suited to PSC studies because they allow measurements to be taken over a greater latitudinal range than the solar occultation method, and also at night (and so within the winter polar regions).

Spang et al. (2001) verified a robust cloud detection method of using the ratio of radiances in the wavenumber ranges of 788–796 cm^{-1} and 832–834 cm^{-1}, which are respectively dominated by CO_2 and aerosol/cloud emissions. Spang et al. (2005) applied this method to the analysis of MIPAS on ENVISAT data, validating the measurements using lidar and satellite data (POAM III and SAGE III). They found that the agreement between the MIPAS and lidar data was very good. The agreement with the other satellite data was also good, although the solar occultation measurements were able to detect optically thinner clouds than the MIPAS measurements. Spang and Remedios (2003) identified a spectral signal at 820 cm^{-1} which they concluded indicates the presence of particles with a high HNO_3 concentration (mass fraction $> 40\,\%$). Höpfner et al. (2006) extended this analysis using refractive indices generated from a number of laboratory studies to generate profiles for the major PSC particle compositions. Using lidar measurements for validation, they demonstrated that dense homogeneous clouds of ice or small (radii $< 3\,\mu$m) NAT particles can be identified using MIPAS measurements.

Satellite-based instruments are important because they allow us to observe large volumes of the atmosphere over several years, so an overview of stratospheric conditions, and estimations of the extent of PSC coverage, can be

made. However, until recently, they could not be used to determine any physical parameters of the aerosols being observed. Even with the information provided by the analysis of extra wavelengths of solar radiation, Strawa et al. (2002) have only been able to distinguish differences in the size of the aerosol particles, and so indirectly determine the type of PSC observed. Because of the scale of these measurements — a typical POAM sample volume is about 200 km long, 30 km wide and 1 km thick — these datasets do not capture well small-scale features.

2.3 Mesoscale Instruments

Most remote measurements of PSCs are made using lidar systems, which, unlike passive sensors, contain a laser source as well as an optical sensor. The laser is aimed towards the area of interest, while the sensor detects the light that scatters at 180°, i.e., directly back towards the instrument. The distance between the lidar and the measurement site is calculated from the time the signal takes to return.

Two properties of the returned signal are measured, the amount of backscattered light and its polarisation, from which are determined the backscatter and aerosol depolarisation ratios. The scattering ratio, S, is the ratio of the total backscatter to the backscatter due to air molecules alone. The ratio of the aerosol backscatter to the molecular backscatter is given by $S - 1$. The total depolarisation ratio, D_T, is the ratio of the perpendicular backscatter return, $R_\perp$, to the parallel backscatter return, $R_\parallel$

$$D_T = \frac{R_\perp}{R_\parallel} \, . \tag{1}$$

The aerosol depolarisation ratio is (Browell et al., 1990)

$$D_a = D_T \frac{S_\parallel (S_\perp - 1)}{S_\perp (S_\parallel - 1)} \,, \tag{2}$$

where $S_\perp$ and $S_\parallel$ are the the scattering ratios for the perpendicular and parallel returns, respectively.

Lidar measurements can be made using a single laser wavelength (e.g., see Poole and McCormick, 1988; Gobbi et al., 1998; Santacesaria et al., 2001), however the amount of information that can be gleaned from the data is greatly increased if two or more wavelengths of light are used (Browell et al., 1990). This allows the use of the colour ratio

$$C(\lambda_2, \lambda_1) = \frac{S(\lambda_2) - 1}{S(\lambda_1) - 1} \,. \tag{3}$$

Two typical wavelengths used for lidar studies are $\lambda_2 = 1.064$ μm and $\lambda_1 = 0.603$ μm. The wavelength dependence of the aerosol backscatter is assumed to be proportional to $\lambda^{-\alpha}$, while molecular scattering is proportional to λ^{-4}. Thus the wavelength dependence of the aerosol backscatter ratio is proportional to $\lambda^{4-\alpha}$. The aerosol backscatter wavelength dependence parameter α is given by

$$\alpha = 4 - \frac{\ln\left(C(\lambda_2, \lambda_1)\right)}{\ln\left(\lambda_2/\lambda_1\right)} \,, \tag{4}$$

and is size dependent. A large α indicates that a majority of particles have radii smaller than the lidar wavelengths, while a small α indicates that the majority of particles have radii larger than the lidar wavelengths (Toon et al., 2000; Shibata et al., 1997).

The aerosol backscatter depends on the particle size distribution, particularly the surface area density, and the particle refractive index, as well as the lidar

wavelength. The amount of depolarisation occurring depends on the shape of the particles. It is small for molecular scattering, and zero for spherical particles, but will occur with even slight departures from spherical shapes. While Mie scattering theory can be used to analyse PSCs consisting of spherical particles (e.g., see Toon et al., 2000), detailed analysis of lidar observations of many PSCs is difficult because they consist of nonspherical solid particles with sizes comparable to the wavelength of the laser. Theoretical modelling can aid analysis; however this must be done by solving the Maxwell equations using numerical techniques (see Liu and Mishchenko, 2001, and references within).

Analysis of lidar data requires knowledge of the purely-molecular backscatter (Browell et al., 1990); lidar measurements are often normalised, therefore, at a high altitude where the signal is assumed to be from molecules alone. However, as discussed by Toon et al. (2000), stratospheric aerosols are ubiquitous, and so data used for normalisation may not be purely molecular. They also noted that aerosol scattering is often not much larger than molecular scattering, and so only considered data for which $S(0.603) > 1.2$ and $S(1.064) > 2.0$ to contain PSCs.

Using the method described above, Browell et al. (1990) identified the existence of two different types of aerosols above the water ice frost point, Types Ia and Ib, and produced a lidar-based classification (Table 1). Toon et al. (1990) used these observations to describe several physical parameters of Type I clouds. The value of α puts limits on the particle size: large values (Type Ib) indicated particles with mode radii less than the laser wavelength, i.e. about $0.5\,\mu$m. Smaller α values (Type Ia) limit the mode radii of the observed particles to $1\,\mu$m or greater. The amount of depolarisation indicates the shape of the particles: the very low depolarisation of the Type Ib particles suggests

that they are almost spherical, while the higher values for the Type Ia particles indicates that they are much less spherical. The backscatter ratio can be used to calculate the total volume concentration of particles. The high value for the Type Ib particles indicates that they have a large volume concentration, and are likely to have taken up most of the atmospheric HNO_3. Conversely, Type Ia particles are likely to have a small total volume concentration. However some non-spherical particles scatter much less efficiently than spheres at 180° so this relationship is less clear cut. Although work has been done on characterising the lidar response to non-spherical particles (Liu and Mishchenko, 2001) and aerosols composed of a number of different particle shapes (Reichardt et al., 2002), this is still a complicated and uncertain field.

Lidar measurements do not provide the compositions of the particles that they detect. To deduce PSC composition, von König et al. (2002) combined lidar measurements of PSCs with gas-phase HNO_3 measurements from the Airbourne Submillimeter Radiometer (ASUR). The ASUR instrument measures radiation at wavelengths of about 0.5 mm, large enough to not be affected by scatter from stratospheric particles, so in the stratosphere the signal is only influenced by absorption by gaseous molecules. By combining the gas-phase HNO_3 measurements with temperature and H_2O data, and lidar observations of PSCs, von König et al. (2002) were able to conclude that the observations in the Arctic on one particular day were consistent with a NAT composition. These observations are limited by the ASUR instrument, which has a vertical resolution of 6–10 km, a horizontal resolution of about 20 km, and a precision of about 0.3 ppb in the lower stratosphere (see von König et al., 2002, and references within). This resolution is good enough for synoptic-scale PSCs, but would not be able to distinguish the thin layering (50–300 m thick) which

has been observed within mesoscale PSCs (Hofmann, 1990).

Remote-sensing instruments can provide measurements of particle shapes and sizes as well as of the total aerosol volume concentration. Combining these with measurements of gas-phase constituents and standard stratospheric number densities allows particle compositions and size distributions to be inferred. However, these measurements are limited by low spatial resolution. For testing microphysical models, the lack of direct composition information is a disadvantage of lidar measurements, but the detailed spatial information is a great advantage (e.g., Tsias et al., 1999; Wirth et al., 1999).

2.4 In-situ Instruments

In-situ instruments cannot provide the same large-scale coverage as remote sensing instruments. However, they do often provide a higher spatial resolution, ca. 100-500m horizontally, allowing the study of small-scale features. To get these instruments up to the stratosphere they can be mounted either on balloons (e.g., Hofmann and Deshler, 1990; Schreiner et al., 2003) or high-altitude aircraft, such as the American ER-2 (e.g., Dye et al., 1992; Northway et al., 2002) and the Russian M-55 Geophysica (e.g., Stefanutti et al., 1999). These platforms have different advantages and disadvantages. Aircraft are very flexible, allowing focused studies of small-scale features. However they have a limited range. Balloons have a potentially far greater range than aircraft, and follow near-lagrangian flight paths, enabling the study of the evolution of air parcels in time. However they can carry fewer instruments, have limited options for steering, and can only be launched when ground-level weather is near calm.

The in-situ instruments most similar to the remote-sensing instruments described above are the backscatter sondes. Backscatter sondes are like lidar but without range detection (i.e. all the backscattered photons from a flash are counted together), and are used to study particles within about 50 metres of the platform. These use backscatter, depolarisation and colour ratios to measure particle shapes and total aerosol volume concentrations in the same way as the lidar systems described above (e.g., see Schreiner et al., 2003; Lowe et al., 2006, and references within).

Optical particle counters, such as the Multiangle Spectrometer Probe (MASP) and Forward Scattering Spectrometer Probe (FSSP), are used to measure the number density and size distribution of the aerosol population. These instruments measure the scattered light produced when individual particles pass through a beam of light (which can be either a laser or white light). The inlets of instruments mounted on aircraft are orientated so that the atmosphere can be passively sampled using the movement of the aircraft, allowing the particles to be measured under near-ambient conditions. Instruments mounted on balloons cannot do this, and so must use pumps to collect samples. Light is scattered in all directions by the particles. All instruments collect the strong forward-scattered signal, though some instruments also collect the weaker back-scattered signal (e.g. MASP, see Drdla et al., 2003, and references within). Mie scattering theory is used to calculate particle sizes, with the assumption that the sampled particles are spherical. In addition, a standard refractive index must be used, usually set to a value between 1.40–1.45, based on an estimation of the average refractive index of stratospheric aerosols. These instruments can typically resolve particles between $\sim 0.2\,\mu$m and $\sim 20\,\mu$m in size. It is also possible to obtain particle number densities. The main limiting

factors on accuracy are uncertainties associated with the sample volume. A statistically significant sample needs to be about 100 particles or more, so sample volumes need to be large to measure the diffuse aerosols present in the stratosphere. This means that sample times can to be up to 2 minutes, resulting in a spatial resolution of 10–20 km for aircraft mounted instruments (Baumgardner et al., 1992).

A chemiluminescence detector for gas-phase NO_y and NO has been mounted on the ER-2 for polar missions since the late 1980s (Fahey et al., 1989). NO_y is the sum of all nitrogen oxides excluding N_2O, i.e., NO, NO_2, HNO_3, etc. In the wintertime lower stratosphere, the majority of NO_y is HNO_3. Recently the instrument has been adapted for measuring large HNO_3-containing particles (Northway et al., 2002). This instrument, which has subsequently been duplicated on the Geophysica (Voigt et al., 2005), has two inlets. The front inlet measures the NO_y and NO content of the gas-phase and all sizes of particles. The rear inlet makes use of particle inertia to avoid sampling any particles larger than $2\,\mu$m aerodynamic diameter. Subisokinetic inlets are used — the internal flow rates are constant and lower than the true speed of the aircraft — which enhance particle number concentrations within the instrument. The factor of enhancement can be calculated using fluid dynamics simulations (Northway et al., 2002), and increases with increasing particle size. By subtracting the NO_y measurement of the rear inlet from that of the front inlet the NO_y content of the large ($> 2\,\mu$m) particles can be measured. When these particles are collected at a lower frequency than the sampling rate (1 Hz) then individual particles can be identified. The size of the individual particles can be calculated using their net NO_y content and assuming a set chemical composition (usually NAT).

The compositions of smaller particles can be measured using the balloon mounted Aerosol Composition Mass Spectrometer (ACMS) (Schreiner et al., 2002). In stratospheric conditions this instrument has a throughput of around 15 $cm^3\ s^{-1}$. The sampled air passes through an aerodynamic lens — which concentrates particles within the size range 0.3–5 μm into a narrow beam — into two vacuum chambers which reduce the air pressure in two steps down to 10^{-8} mbar, used to produce an enhanced aerosol-to-gas signal ratio within the mass spectrometer. Particles take about 0.5 ms to pass through the vacuum chambers. Model calculations and experimental results show that the change in composition of particles larger than 0.1 μm during this time is negligible (Schreiner et al., 2002). From the vacuum chambers the aerosol beam passes into an evaporation sphere, which is heated to 80 °C. Finally the majority of the resulting gas enters the mass spectrometer to be measured, while approximately 30 % of the particle mass is lost back to the vacuum chamber. The background signal of the instrument due to the remaining part of the gas-phase can be determined by moving the focus of the lens away from the evaporation sphere, stopping any particles from entering the sphere and so being measured. The relative count rates of the different chemical species measured, typically H_2O and HNO_3, allowing particle composition to be determined. However the sizes and number of particles measured cannot be reliably determined due to the mixing of the signals from different particles and the loss of mass from the evaporating sphere.

3 Particle Compositions

Since the discovery of PSCs, a number of different types of particles have be postulated as as being important in the formation and lifecycles of these aerosols. Observations of PSCs have been split into Types Ia, Ib and II based on classifications of lidar measurements (Poole and McCormick, 1988; Toon et al., 1990). However these divisions are based on the optical parameters of the aerosols, which, while providing an idea of typical shapes and sizes of particles, contain very little information about the actual composition of the particles. Below we will discuss the current ideas on the compositions of, and transitions between, the different types of PSC particles. The broad lidar classifications will be used to provide a loose structure; however on occasions we will stray outside these limits.

3.1 Type Ib particles

Because of their particle sizes and shapes, Type Ib PSCs are believed to consist mostly of STS droplets. These are formed by the condensational growth of the background stratospheric aerosol, which is comprised of binary H_2SO_4/H_2O particles (Rosen, 1971). The amount of sulphuric acid in the condensed phase increases significantly as the temperature decreases from ~ 240 to $\sim 210\,\mathrm{K}$ (Figure 5). For temperatures of 200 K and below it can be assumed that all the sulphuric acid is in the condensed phase. This makes changes in the compositions of the binary particles easier to calculate, because only transport of water from/to the vapour phase need be considered. The mass fraction of H_2SO_4 in the droplets decreases with decreasing temperature, because of the

extra water vapour which is taken up by the particles. The first parameterisation for the composition and volume of stratospheric H_2SO_4/H_2O aerosols was developed by Steele and Hamill (1981).

There are several other gaseous species which will dissolve into the stratospheric H_2SO_4/H_2O droplets, including the halogen "reservoir" species: HCl, HBr, HOCl and HOBr. Halogen compounds may react in the liquid aerosol to release photochemically active species which catalytically destroy ozone (Solomon, 1990, 1999). Thermodynamical models have been developed to model the equilibrium properties of liquid stratospheric droplets (e.g. Carslaw et al., 1994; Cox et al., 1994; Tabazadeh et al., 1994). The models show a rapid change in particle composition about 4–5 K above the ice frost point, from almost binary H_2SO_4/H_2O solutions to almost binary HNO_3/H_2O solutions (Figure 6). At these temperatures, the majority of HCl and HBr in the system transfers to the condensed-phase (Fig. 6a). However these species are much less abundant than HNO_3, and so are only minor constituents of droplets (Fig. 6b).

Particles do not always maintain equilibrium with the atmosphere. For example, Peter et al. (1994) noted that NAT particles take several hours to re-equilibrate with the gas-phase after undergoing a rapid change in conditions. In the case of crystalline particles, such as NAT or SAT, with a fixed composition, this process merely entails a change in the mass of the particle. Liquid particles, on the other hand, do not have a fixed composition. Thus, in theory, they can adopt very different compositions during this re-equilibrium process from that which would be the case if equilibrium was maintained. Using a microphysical model, Meilinger et al. (1995) investigated the behaviour of an ensemble of STS droplets subjected to rapid temperature changes. They

found that, during rapid cooling, the majority of the particles in the distribution would not take up HNO_3 rapidly enough to remain in equilibrium with the atmosphere. The resulting increase in the HNO_3 saturation ratio allows the smallest particles to overcome the Kelvin effect and rapidly grow, gaining a far higher HNO_3 mass fraction than would otherwise occur (Figure 7). The hysteresis effect observed in the evolution of the HNO_3 mass fraction occurs because HNO_3 is a factor of $\sim$500 less abundant than H_2O in the stratosphere. The time taken for a particle constituent to regain equilibrium with the gas-phase is dependent on the particle size and partial pressure of the constituent. Thus, after an infinitesimal temperature change, the time taken for HNO_3 in a particle to regain equilibrium with the gas-phase is 7 hr and 10 min, for particles of radius 2 and 0.1 μm, respectively. For H_2O the time lag decreases to 29 s and 0.7 s, respectively (Meilinger et al., 1995).

Figure 8 demonstrates the importance of non-equilibrium compositions. The data shown (diamonds) are from a balloon flight from Kiruna, Sweden, on 25 January 1998 (Schreiner et al., 1999), and show $HNO_3 : H_2O$ mole ratios from mass-spectrometer measurements in a PSC. The data clearly do not fall on the equilibrium STS composition, even considering a range of possible gas-phase abundances of HNO_3. Using a non-equilibrium model for the growth of the liquid PSC droplets (Lowe et al., 2003) captures much more of the observed variability on composition. As expected from the relaxation time arguments, above, the non-equilibrium particles are usually deficient in HNO_3, by up to a factor of three at $T - T_{ice} \approx 4$ K, for example. Such disequilibrium in mountain-wave PSCs has also been observed in aircraft measurements (Lowe et al., 2006).

SAT particles are not directly related to observations of Type Ib PSCs; they

are, however, the thermodynamically stable form of H_2SO_4/H_2O particles between 188–213 K (Koop and Carslaw, 1996). Thus we must consider their possible effects on the growth of STS droplets from the background sulphate particles. SAT is a crystalline solid with the chemical composition $H_2SO_4 \cdot 4H_2O$. It is part of a broad family of crystalline sulphuric acid hydrates, which includes the monohydrate, SAM ($H_2SO_4 \cdot H_2O$), the hemihexahydrate, SAH ($H_2SO_4 \cdot 6.5H_2O$) and and the octahydrate, SAO ($H_2SO_4 \cdot 8H_2O$).

Koop and Carslaw (1996) studied the stability conditions for H_2SO_4 solid phases by comparing the composition of stratospheric H_2SO_4/H_2O droplets with the melting points of the different solid phases (Figure 9). A useful measure of the stability of the solid phases is their saturation ratios in an atmosphere of the relevant composition. When these are greater than 1 then the solid is stable, less than 1 and the solid is unstable. From Figure 9B we would deduce that SAT particles form ice particles below 188 K (point c). Figure 9A also suggests that SAT particles should change to different solid phases when the temperature increases above point (a). However, laboratory experiments have shown that SAT will melt rather than change to a different solid phase when warmed above 210–215 K (Middlebrook et al., 1993).

As discussed above, liquid stratospheric aerosols absorb large amounts of HNO_3 at low temperatures (Zhang et al., 1993; Molina et al., 1993), which will change the behaviour of stratospheric SAT particles when cooled. The stability of dry SAT particles can be determined by examining the saturation ratio in liquid droplets with the same composition as SAT under the same atmospheric conditions (Figure 10). The addition of HNO_3 to the system significantly reduces the stability of SAT, which deliquesces simply because it is less thermodynamically stable than STS. However experimental results (Iraci et al., 1998)

indicate that this process may be kinetically limited. Only $\sim 60\%$ of SAT samples subjected to conditions below the critical temperature of deliquescence (point 1 in Figure 10) exhibited SAT loss to form $HNO_3/H_2SO_4/H_2O$ solution.

The composition and stability conditions for SAT, as well as its phase transitions to aqueous H_2SO_4 and HNO_3 solutions, are well known. However the formation routes for SAT are more obscure. Laboratory experiments (Middlebrook et al., 1993; Beyer et al., 1994; Koop et al., 1997b) have not observed the homogeneous nucleation of SAT above the ice point, which, with the addition of an analysis of nucleation statistics (Koop et al., 1997b), suggests that sulphate aerosols do not freeze homogeneously to form sulphuric acid hydrates. Laboratory experiments (Bogdan et al., 2003) also found that concentrated (>40 wt% H_2SO_4) sulphate droplets will not heterogeneously freeze on silica particles at stratospheric temperatures. It has been suggested that liquid H_2SO_4/H_2O droplets may behave like glassy solids below ~ 194 K and crystallize upon warming to form SAT (Tabazadeh et al., 1995). However Koop et al. (1997b) showed that the rate of crystal growth is such that stratospheric aerosol droplets would freeze as soon as nucleation has occurred. In laboratory work, SAT is formed using supercooling, a process which invariably also produces water ice. Thus it is likely that SAT heterogeneously nucleates on other crystalline solids in the stratosphere; however no studies of nucleation rates have been made.

3.2 Type II particles

Type II PSCs were identified as consisting of large ($\geq 10\,\mu$m) crystalline particles which only exist below the stratospheric ice frost point of ~ 188 K (Poole

and McCormick, 1988). The obvious choice of composition for these particles is water ice (Turco et al., 1989). However, because these ice crystals nucleate from HNO_3-rich particles, the compositions and lifecycles of these particles must be more complicated than those of pure H_2O ice crystals.

Three routes of ice formation have been suggested: vapour deposition of ice onto either SAT or NAT, homogeneous nucleation from an aqueous solution, and heterogeneous nucleation in aqueous solutions containing solid cores. Vapour deposition of ice onto NAT particles was postulated as a method of formation for Type II particles while the three-stage model of PSC formation was in favour (e.g. Hanson and Mauersberger, 1988; Peter et al., 1991). However no studies have been made into this route of formation. Recent experimental work into the vapour deposition of ice on to SAT has observed ice formation at supercoolings of $\leq 1\,\mathrm{K}$ below the ice frost point (Fortin et al., 2003). However this route would require the existence of SAT below its deliquescence temperature. This may occur for up to $\sim$40% of the available SAT particles (Iraci et al., 1998), but is more likely when the majority of the available HNO_3 has been taken up into NAT particles (lowering the deliquescence temperature).

With the addition of STS to the list of possible PSC particles, the homogeneous nucleation of ice from STS was proposed. Laboratory experiments with solutions such as H_2SO_4/H_2O, HNO_3/H_2O and $HNO_3/H_2SO_4/H_2O$ have shown that homogeneous nucleation of ice requires the solution to be supercooled 2–3 K below the ice frost point (e.g., Chang et al., 1999; Koop et al., 1998; Middlebrook et al., 1993). Theoretical studies, using classical homogeneous freezing theory, are consistent with this (MacKenzie et al., 1995, 1997, 1998). Using experimental data Koop et al. (2000) developed a thermody-

namic scheme for homogeneous ice nucleation, expressed as a function of the water activity and pressure. These experiments and theories have assumed that the ice nuclei would form within the interior volume of the droplet. However Tabazadeh et al. (2002b) proposed that the gas-liquid interface may be important for homogeneous freezing of atmospheric droplets. The relative importance of surface- and volume-based nucleation within their scheme depends on the temperature and size of the droplet. Smaller droplets are more likely to undergo surface nucleation, while lowering the temperature increases the likelihood of volume-based nucleation occurring. A recent laboratory study (Duft and Leisner, 2004) has demonstrated that homogeneous freezing in water droplets with radii 19–49 μm is volume-based, although further study is required to discover if this is true for smaller droplets. Computational simulations (Vrbka and Jungwirth, 2006) suggest that, during homogeneous freezing, ice nuclei are more likely to form within the sub-surface region. They suggest this is because the change in volume associated with freezing is more easily accommodated near the surface than in the bulk of the liquid. However, the disorder of the immediate liquid surface is not conducive to crystal formation. Liquid PSC particles are not pure water, so the water droplet simulations are not directly applicable to PSCs, and it has been noted that the surface of an aqueous particle is often enriched with chemical components such as nitric acid, making it more difficult for an ice nucleus to form at the surface of such a particle (see Tabazadeh et al., 2002b, and references within).

Theoretical work on heterogeneous nucleation of ice particles from aqueous solutions in the troposphere suggests that this process could be important for the formation of cirrus clouds in the northern hemisphere (e.g., see Gierens, 2003, and references within). However, the total abundance of condensation

nuclei is far less in the lower stratosphere, 10–60 cm^{-3}, than in the upper troposphere, 600–1600 cm^{-3} (Sheridan et al., 1994), and it is believed that only a fraction of these are likely to act as ice nuclei. From this we might infer that heterogeneous ice nucleation is less relevant in the stratosphere, although recent laboratory experiments have shown that fumed silica can act as a nucleus for the heterogeneous freezing of ice from dilute ($\sim 7\%$ HNO_3) nitric acid solutions (Bogdan et al., 2003). Since fumed silica is similar in composition, and method of formation, to meteoritic smoke particles, then these particles, which have a number concentration of 100 cm^{-3} in the stratosphere, could act as heterogeneous nuclei for ice particles (see Bogdan et al., 2003, and references within).

The equilibrium partitioning of H_2O between the solid and gas phases for a water ice particle can be calculated using, for example, the empirical equation derived by Marti and Mauersberger (1993). STS particles are, however, not composed purely of water, and so the ice freezing process must take account of the other chemical constituents of the droplet. One possibility is that the other components of the droplet, in this case mostly HNO_3 and H_2SO_4, could simply be adsorbed onto the surface of the ice particle as it grows, and become embedded in the ice matrix without forming hydrates. However the thermodynamic solubilities of HNO_3 and H_2SO_4 in ice are of the order of parts per million (Davy and Somorjai, 1971), at least five orders of magnitude less than their mixing ratios in PSCs. Instead it is likely that the remaining part of the original STS will form either solid NAT/SAT or a liquid STS layer on the surface of the ice particle.

Using the thermodynamic model of Carslaw et al. (1995), Koop et al. (1997a) investigated the stabilities of the different possible PSC phases. They found

that liquid solutions can co-exist with both NAT and ice, provided that H_2SO_4 remains in the aqueous phase. Liquids in equilibrium with a solid phase consisting just of ice contain $\sim 40\,\mathrm{wt\%}$ HNO_3 and trace H_2SO_4, whilst equilibrium with NAT would result in a H_2SO_4-rich solution. Liquids in equilibrium with SAT would have HNO_3 vapour pressures in excess of the total available HNO_3, and so are thermodynamically unfeasible. So a Type II particle is likely to consist of a combination of different chemical phases, with typically combinations being: ice/STS, ice/NAT/STS (almost binary H_2SO_4/H_2O solution), and ice/NAT/SAT.

3.3 Type Ia particles

Type Ia particles are classified as medium-sized ($\geq 1\,\mu\mathrm{m}$) aspherical particles, which can exist several degrees above the ice frost point (Toon et al., 1990). Their aspherical shape implies that they are solid particles, most likely nitric-acid hydrates. Experimental work by Hanson and Mauersberger (1988) demonstrated that the stable nitric-acid hydrate under stratospheric conditions is nitric acid trihydrate (NAT, $HNO_3{\cdot}3H_2O$, $\sim 54\,\mathrm{wt\%}$ HNO_3), which can exist up to about 7 K above the ice frost point. Later experiments by Worsnop et al. (1993) showed that other nitric-acid hydrates are metastable under stratospheric conditions (Figure 11). They suggested that nitric acid dihydrate (NAD, $HNO_3{\cdot}2H_2O$, $\sim 64\,\mathrm{wt\%}$ HNO_3) would form readily in the stratosphere and could persist for several days; a conclusion which is supported by recent studies into NAD crystalline structures and formation routes (Natsheh et al., 2006). This tendency to nucleate metastable phases may indicate a relatively high free-energy barrier for nucleation of NAT compared

with other crystalline nitric-acid hydrates (Worsnop et al., 1993). Although the existence of nitric-acid hydrates in the polar winter stratosphere has been known to be possible since the mid-1980s, it has only been recently that direct in-situ measurements of particle compositions have confirmed the existence of NAT particles in the stratosphere (Voigt et al., 2000a). No direct stratospheric measurements of NAD particles have been made.

As with stratospheric ice particles, there have been three routes of formation suggested for HNO_3 hydrates: vapour deposition onto either ice or SAT, homogeneous nucleation from an aqueous solution, and heterogeneous nucleation in aqueous solutions containing solid cores. The original three-stage model of PSC formation implied that NAT would nucleate directly from the gas-phase on to SAT particles. However, theoretical studies cast doubt on this mechanism (MacKenzie et al., 1995), and laboratory studies (Iraci et al., 1995) showed that the formation of NAT on SAT is strongly hindered up to NAT saturation ratios of 127, implying that this process is kinetically very unlikely in the stratosphere. A possible exception to this is when SAT surfaces have been primed for NAT nucleation by a previous deposition-and-evaporation cycle of NAT on the surface (Zhang et al., 1996). This process could occur in the stratosphere for SAT particles which originally formed as part of a multiphase particle which included NAT, but the formation route for these particles is uncertain. In addition, the NAT saturation ratios needed for deposition onto SAT occur below the deliquescence temperature of SAT in the stratosphere.

Bulk freezing experiments (Koop et al., 1997b) showed that the nucleation of NAT from binary HNO_3/H_2O solutions containing ice particles occurred faster if the ice particles had passed through the gas-phase first. Koop et al. (1997b) interpreted this to mean that NAT/NAD had nucleated heterogeneously from

the gas phase on to the ice particles while they were sedimenting. When the crystals reached the liquid they seeded NAT and ice formation in the binary solution. The nucleation of NAT by vapour deposition onto ice surfaces has been observed at high NAT supersaturations (Biermann et al., 1998; Middlebrook et al., 1996). Modelling studies (Luo et al., 2003) have suggested that rapid cooling within gravity waves would suppress the growth of STS particles, allowing the development of large NAT saturation ratios in parallel with the growth of ice particles (Figure 12). This could result in the nucleation of NAT onto the ice particles, which would then persist as NAT particles after the ice had evaporated away (Luo et al., 2003).

The most direct method of NAT formation would be homogeneous freezing from STS droplets. However there are severe limitations. Bulk freezing experiments (Koop et al., 1995, 1997b) demonstrated that the presence of $\geq$0.1 wt% H_2SO_4 would lower the freezing temperatures of $HNO_3/H_2SO_4/H_2O$ solutions by $\geq$10 K below those typical of HNO_3/H_2O solutions. Bertram et al. (1996); Disselkamp et al. (1996), and Bertram and Sloan (1998) found somewhat different results while studying the freezing of 1:2 (HNO_3:H_2O molar ratio) nitric acid aerosol droplets to NAD. Freezing in the experiments of Disselkamp et al. (1996) produced NAD much more easily from solutions with a HNO_3:H_2O molar ratio of 1:2 than NAT from solutions with a molar ratio of 1:3 (the nucleation rates differ by a factor of 10^3 or more). Freezing temperatures in the experiments of Bertram et al. (1996); Bertram and Sloan (1998) were some 20 K below those in the Disselkamp et al. (1996) experiments. It is not clear why these experimental results are so different. Classical freezing theory — that is also consistent with NAT, SAT, and ice freezing experiments — is consistent with the Bertram et al. (1996); Bertram and Sloan (1998) re-

sults (MacKenzie et al., 1998). Subsequent empirical fits to laboratory results (Möhler et al., 2006) fit the results of the most recent study (Stetzer et al., 2006) and those of the earlier studies, using a fitted version of classical freezing theory.

As discussed previously, Meilinger et al. (1995) suggested that these limitations might be overcome during the rapid changes in conditions which occur within gravity waves. However the maximum HNO_3 mass fraction they reported was $\sim$52% in cooling rates of up to $36\,\mathrm{K\,hr^{-1}}$, which is close to the NAT stoichiometry, but not that of NAD. Tsias et al. (1997) expanded on this work, examining the effect of faster temperature changes on the droplet compositions. They found that particles could reach HNO_3 mass fractions of $\sim$58% ($\sim$1:2.5 HNO_3/H_2O) during warming at rates of $\geq 100\,\mathrm{K\,hr^{-1}}$ (temperature change rates in stratospheric mountain wave events can be up to $150\,\mathrm{K\,hr^{-1}}$, e.g. see Tsias et al., 1997, and references within). They demonstrated experimentally that binary HNO_3/H_2O droplets of similar compositions would freeze to NAD typically within one hour. During mountain wave events, however, such compositions are only achieved for a few minutes, so only a small fraction of the droplets at such compositions (which would be a small fraction of the total aerosol population) would freeze.

Experimental studies of binary HNO_3/H_2O droplet freezing (Salcedo et al., 2000, 2001) were extrapolated linearly to stratospheric conditions and used to hypothesise a "nucleation window" for the production of NAD (Tabazadeh et al., 2001). Such a linear extrapolation is forbidden by thermodynamics (Knopf et al., 2002) and particle production rates (for NAT and NAD) are much smaller than those predicted by Tabazadeh et al. (2001) (Figure 13b).

While all of the studies above have assumed that homogeneous nucleation would occur within the bulk of a liquid, other work (Tabazadeh et al., 2002a,b) has proposed surface-based nucleation. In this process, the nucleating solid reduces the energy needed to form a stable crystal by forming part of its surface out of the liquid, in contact with the gas-phase. This method is only favoured in cases where the solid is partially (but not fully) wettable by its own liquid melt. Tabazadeh et al. (2002a) re-analysed data from laboratory studies of the freezing of NAT and NAD from binary HNO_3/H_2O solutions using a formulation for surface-based nucleation. They found that the formulation for surface nucleation fitted the data better than the volume-based formulation and is, at least in the case of NAD nucleation, less temperature dependent. A comparison of atmospheric NAD production rates derived using the two formulations (Figure 14), show that the surface-based production rate is $\sim 10^2$ greater than the volume-based production rate used in their earlier work (Tabazadeh et al., 2001). Applying the factor of 10^2 to the stratospheric production rate of NAD of Knopf et al. (2002) (as shown in Figure 13b) we only obtain a production rate of $\sim 10^{-11}\,\mathrm{cm}^{-3}\,\mathrm{hr}^{-1}$. This is still much smaller than the production rates of $10^{-5}\,\mathrm{cm}^{-3}\,\mathrm{hr}^{-1}$ that microphysical sensitivity studies suggest are needed for homogeneous nucleation to have a significant influence on the overall number of HNO_3-hydrate particles in the stratosphere (Tabazadeh et al., 2001). Recently Stetzer et al. (2006) have demonstrated that their measurements of freezing rates of NAD from small (0.25μm) binary HNO_3 droplets, in the low temperature aerosol chamber AIDA, agree well with the results of a number other freezing studies in the literature when using volume-based nucleation rates. The surface-based nucleation rates Stetzer et al. (2006) obtained from their data were also 1–3 orders of magnitude lower than those calculated by Tabazadeh et al. (2002a). They concluded that, for

binary HNO_3 droplets, volume-based, rather than surface-based, homogeneous nucleation is more likely under stratospheric conditions. Their companion paper (Möhler et al., 2006) estimates very small homogeneous (volume-based) nucleation rates for NAT in the stratosphere.

When considering liquid particle microphysics, we need to take into account the surface enrichment of HNO_3 in both binary HNO_3/H_2O and ternary $HNO_3/H_2SO_4/H_2O$ solutions (Yang and Finlayson-Pitts, 2001; Donaldson and Anderson, 1999), which could influence surface-based nucleation rates. In addition, the presence of H_2SO_4 in STS droplets can strongly inhibit the nucleation of HNO_3-hydrates (Koop et al., 1997b). The Koop et al. (1997b) experiments, however, used bulk samples, which are not suitable for studying surface-based nucleation. Tabazadeh et al. (2002a) have suggested that, if H_2SO_4 is not a "surface active" component, then it will have little effect on the surface tension of the solution, and so on the free energy barrier to nucleation. However more measurements of the nucleation of NAT/NAD in ternary solution droplets, at stratospherically relevant temperatures, are needed in order to answer these questions. In conclusion it appears that, from current knowledge, homogeneous nucleation of NAT/NAD from STS is not significant in the stratosphere, although there is not universal consensus on this subject.

As mentioned above, bulk freezing experiments (Koop et al., 1997b) have shown that heterogeneous nucleation of NAT from nitric-acid solutions on to ice is too slow a process to be significant in the stratosphere. In addition, laboratory measurements (Zondlo et al., 2000) indicate that binary HNO_3/H_2O solutions on an ice surface do not nucleate to NAT readily, but form a metastable liquid HNO_3/H_2O film instead.

Laboratory experiments using finely divided aqueous systems (Bogdan et al., 2003) have shown that binary HNO_3/H_2O solutions with $\sim 53\,\mathrm{wt\%}$ HNO_3 will heterogeneously freeze to nitric acid hydrate on fumed silica at around 195 K. These results suggest that heterogeneous nucleation of NAT/NAD on meteoritic smoke nuclei could occur on STS particles passing through gravity waves, in a similar manner to the non-equilibrium homogeneous freezing described above. Similar experiments with binary H_2SO_4/H_2O solutions found that freezing did not occur until around 175–180 K, too low a temperature for the stratosphere. This suggests that, again in a similar manner to homogeneous freezing of STS (Koop et al., 1997b), the heterogeneous freezing of liquid PSCs will only occur when H_2SO_4 is a minor constituent of the droplets ($\leq 0.1\,\mathrm{wt\%}$), although only freezing experiments with ternary $HNO_3/H_2SO_4/H_2O$ solutions will prove this theory.

4 The effects of PSCs

Soon after the discovery of the ozone hole PSCs were found to be important both for aiding the release of active chlorine species as well extending the lifetimes of these species by removing HNO_3 (Toon et al., 1986; Solomon et al., 1986; Solomon, 1990, 1999).

Below we review how the microphysical properties of the PSCs determine the magnitude and extent of these effects, and how the microphysical properties are, in turn, dependent on the climate of the polar vortex. The Antarctic vortex is generally more stable, with greater symmetry around the pole, than the Arctic vortex. This is due to the more disruptive atmospheric wave activity in the Northern hemisphere, which is caused by the configuration of land and

sea in that hemisphere (see, e.g., Solomon, 2004, for a succinct description). As a result, the temperature distribution, and so volume of the air in which PSCs can exist, of the Arctic vortex depends greatly on the dynamical situation of each winter (Pawson and Naujokat, 1999). As a consequence chlorine is frequently fully activated within the Antarctic vortex and so ozone loss is large (e.g. WMO, 2006). Ozone loss within the Arctic vortex can vary considerably from year to year, and is very dependent on changes in climate conditions (Rex et al., 2004). The interactions between stratospheric ozone and climate are outside the scope of this review — the interested reader is directed to WMO (2006); Eyring et al. (2005) and references therein — but we note in passing that global warming at the surface is associated with cooling in the stratosphere. This is because greenhouse gases trap terrestrial infrared near the Earth's surface and reduce the flux entering the stratosphere. There is evidence that the volume of Arctic stratosphere susceptible to ozone destruction may be changing, particularly in those years that are generally cold (Rex et al., 2004).

Lidar observations of PSCs from Ny-Ålesund and McMurdo are illustrative, though not representative, of the differences in current PSC climatology between the two hemispheres (Maturilli et al., 2005). The number of days with PSC observations was found to be 5 times higher at McMurdo (78°S, 167°E) than at Ny-Ålesund (79°N, 12°E). PSCs above McMurdo generally contained NAT, with very few observations of liquid or ice particles. In contrast, liquid PSCs were more common than NAT PSCs above Ny-Ålesund, however almost two-thirds of the days on which PSCs were observed both liquid and NAT PSCs were present.

Below we will examine the current knowledge of how the microphysics of PSC

particles affect heterogeneous reactions, and their role in removing HNO_3. We do not undertake a discussion of stratospheric chemistry in general; this can be found in, e.g. Brasseur and Solomon (2005); Seinfeld and Pandis (2006); MacKenzie (2003). Detailed discussions of outstanding problems in stratospheric chemistry are given in the special issue of *Chemical Reviews* on long-term issues in atmospheric chemistry (Ravishankara , 2003).

4.1 Heterogeneous Reactions on PSC particles

Investigation into the properties of PSCs has been driven by their role in the destruction of the ozone layer. It was Farman et al. (1985) who first highlighted the thinning of the Southern polar ozone layer during the austral spring. Solomon et al. (1986) demonstrated that ozone depletion was confined to the lower polar stratosphere (10–20 km), which McCormick et al. (1981) had shown to contain PSCs during the austral winter. Solomon et al. (1986) proposed two new heterogeneous reactions which, taking place on the surfaces of PSC particles, would release active halogen species, principally Cl_2, from inert reservoir species:

$$\mathrm{XONO_2(g) + HY(s,l) \rightarrow XY(g) + HONO_2(s,l)}, \quad (5)$$
$$\mathrm{XONO_2(g) + H_2O(s,l) \rightarrow HOX(g) + HONO_2(s,l)}. \quad (6)$$

where X and Y can be either Cl or Br. The photolytically active gaseous molecules, XY and HOX, resulting from reactions 5 and 6, as well as the reaction

$$\mathrm{HOX(g) + HY(s) \rightarrow XY(g) + H_2O(s)}, \quad (7)$$

would release atomic chlorine or bromine with the onset of spring, initiating the catalytic destruction of ozone (Solomon, 1999).

The rates of reactions 5–7 due to the interaction of gas and aerosol can be represented by the molecular flux J

$$J = \gamma n_g \bar{c}/4, \tag{8}$$

where γ is the uptake coefficient, n_g is the density of the gas species and $\bar{c}$ is the mean gas molecular speed. J depends on a number of processes: gas-phase diffusion, mass accommodation, Henry's law solubility (in the case of liquids), chemical reactions in the condensed bulk phase, and particle surface properties. These processes are coupled to each other, making their individual determination from laboratory data difficult. Instead, in reactive uptake cases, γ can be approximated by

$$\frac{1}{\gamma} = \frac{1}{\alpha} + \frac{1}{\gamma_{sol} + \gamma_{rxn}}, \tag{9}$$

where α is the mass accommodation coefficient for the relevant species, γ_{sol} is the solubility uptake coefficient, and γ_{rxn} is the reactive uptake coefficient. In cases of low solubility, or long exposure time, the system reaches a steady state and γ_{sol} becomes negligible; γ comes to be governed by α and γ_{rxn}.

Uptake coefficients for many of the different permutations of reactions 5–7 on typical stratospheric aerosol types have been derived using laboratory data. State of the art values for these are documented in the reviews published by JPL and IUPAC (respectively available from http://jpldataeval.jpl.nasa.gov and http://www.iupac-kinetic.ch.cam.ac.uk). Experimental results indicate that uptake coefficients for most combinations of reactions 5–7 on water ice are

less than 0.3 (Sander et al., 2006). Experimental results indicate similarly small uptake coefficients for reactions on nitric acid ice, although parameterisations are only available for the reactions $ClONO_2 + H_2O$, $ClONO_2 + HX$, and $HOCl + HCl$. Studies of reactions 5–7 on sulphuric acid solutions have shown a strong negative temperature dependence — caused by the dependence of these reactions on the solubility of the halogen species and on the activity of H_2O, which have inverse relationships with temperature. The most recent, and comprehensive, parameterisation of reactions 5–7 for chlorine species is given in Shi et al. (2001). Looking at their parameterisation we see that the uptake coefficients for all the reactions increase as the temperature decreases (and the H_2SO_4 mass fraction drops), until just under 50% H_2SO_4, when reaction 5 wins out in the competition with the other two reactions and approaches unity, while the other reactions don't get above 0.1 (Figure 15). Reactions 5 and 6 have been parameterised for chlorine over SAT (Zhang et al., 1994a), however no more parameterisations are available for reactions occurring on SAT, likewise for reactions occurring on STS. Instead, for STS droplets, current microphysical models use the reaction rates for binary sulphuric acid droplets (e.g. Drdla and Schoeberl, 2003).

The activation rates of halogens on aerosol particles are influenced by both the uptake coefficient on the particle and the particulate surface area available. Although we do not have measured values for all these reactions on all possible stratospheric aerosol types, we can see that, for the temperatures at which PSCs exist, the uptake coefficients are much greater for the background stratospheric liquid sulphate aerosols than for the solid PSC particles. The available surface area of the liquid sulphate aerosol is generally much higher than that of the solid PSCs – the mean background stratospheric aerosol sur-

face area density is $1\mu m^2 cm^{-3}$ (e.g. Thomason et al., 1997) – but very much less than the surface area density of liquid PSCs. Within the stable Antarctic vortex, NAT PSCs with relatively large surface area densities are widespread; in the Arctic vortex, however, such dense NAT PSCs tend to be limited to the relatively small cold regions induced by mountain waves (e.g. Carslaw et al., 1998b; Toon et al., 2000). Water ice PSCs are even less common, due to their low formation temperatures, however when they do form they can provide aerosol surface areas 100 times greater than those of liquid or NAT PSCs (e.g. Carslaw et al., 1998b).

Since the onset of chlorine activation occurs at $\sim$ 195 K (Toohey et al., 1993; Webster et al., 1993), it was initially assumed that activation was due to type I (i.e. NAT) PSCs. As knowledge of PSC microphysics has improved it has become clear that chlorine activation is due more to the presence of liquid rather than NAT particles. However, as a first order approximation, many large-scale simulations of stratospheric ozone loss still use T_{NAT} or 195 K as the threshold temperature for switching on heterogeneous chlorine activation (e.g. Kühl et al., 2004; Geer et al., 2006). Drdla (2007) suggests that the coincidence of chlorine activation with T_{NAT} occurs because at standard stratospheric conditions this also happens to be close to the temperature at which chlorine activation becomes significant on the background liquid sulphate aerosols. However this relationship can break down in air masses which have under gone perturbations such as denitrification. Drdla (2007) have developed a parameterisation (called T_{ACL}) — based on H_2O mixing ratio, sulphate surface area at 210 K, and pressure — which can be used as a diagnostic of where chlorine activation is most likely. Finding a sufficiently accurate and computationally efficient parameterisation of PSCs and chlorine activation for global-scale

models is one of the most important remaining problems in PSC studies.

As noted above, current microphysical models which deal with chlorine activation on STS droplets must use reaction rates devised for sulphuric acid solutions. Measurements of reactions 5–7 on ternary have been made, but no clear parameterisation has been produced. Zhang et al. (1994b) measured reactions 6 and 7, and concluded that the rates of these reactions were unaffected by the presence of HNO_3. However none of their solutions contained more than 5% HNO_3. Elrod et al. (1995) measured reaction 6 over ternary solutions with HNO_3/H_2SO_4 mass fractions between 0.283/0.202 – 0.022/0.503. The reaction probabilities they measured for these solutions were between 5–32% lower than those they measured for sulphuric acid solutions at representative compositions for the relevant stratospheric temperatures. However there was no obvious dependence on composition in these reductions. Zhang et al. (1995) measured Reaction 5 on ternary solution over the temperature range 196–214 K. The HNO_3/H_2SO_4 mass fractions at 196 K were 0.112/0.364 (as calculated by Hanson, 1998). They concluded that the probabilities of Reaction 5 were the same for ternary solutions as they were for sulphuric acid solutions; however Hanson (1998) noted that, where appreciable amounts of HNO_3 are present, their data are consistent (within uncertainties) with a significant reduction in the reaction probabilities. Hanson (1998) measured Reactions 5 and 6 on ternary solutions with HNO_3/H_2SO_4 mass fractions of 0.044/0.446 to 0.256/0.203. They found that the measured reaction probabilities were significantly lower than those predicted for the corresponding sulphuric acid solutions. Fits to the data were obtained by reducing the bulk reaction probability by a factor of 2, and the surface reaction probabilities by a factor of 0–10 (increasing with increasing HNO_3 mass fraction). However they

produced no comprehensive parameterisation of the reaction probabilities on ternary solutions.

To date there have been no more experimental investigations of the rates of reactions 5–7 on ternary solutions. The lack of data on these reactions is hampering our understanding of chlorine activation in the Arctic vortex, where STS PSCs are very common (e.g. Maturilli et al., 2005). The increases in particle surface area of STS aerosols over sulphuric acid aerosols, due to the uptake in nitric acid and water, will lead to a greater activation of chlorine. However this increase may not be as large as that currently seen in microphysical models if the presence of HNO_3 reduces the reaction rates by the degree seen in the studies of Elrod et al. (1995) and Hanson (1998)(Lowe et al., 2006).

4.2 Denitrification

In addition to providing reactive surfaces for the release of active chlorine compounds, PSCs can contribute to the destruction of ozone via the denitrification of the stratosphere. The condensation of HNO_3 on to PSC particles stops the deactivation of gas-phase $ClO_x$by reaction with NO_2 from photolysed HNO_3 (Toon et al., 1986). If PSC particles subsequently sediment out of the stratosphere, then the HNO_3 they contain is permanently removed, extending the lifetime of the active chlorine compounds. Denitrification occurs in both polar stratospheres (e.g. Fahey et al., 1990), however it is most intense over Antarctica; where large fractions of the total HNO_3 are irreversibly removed.

The differences in the amounts of denitrification, and ozone loss, between the two hemispheres are due to the greater stability of the Antarctic vortex. Al-

though both vortices form at similar times in the autumn/early-winter, on average the Antarctic vortex breaks down a month later in the season than the Arctic vortex. In addition, while the Antarctic vortex is generally very stable except during the spring breakup; the area, position, and strength of the Arctic vortex are highly variable, especially during the late winter (Waugh and Randel, 1999). The stability of the Antarctic vortex produces much colder conditions than are experienced in the Arctic stratosphere, allowing increased PSC formation which leads to greater denitrification. In addition, extending the cold stratospheric temperatures into the austral spring allows the reactivation, on PSCs, of any $ClONO_2$ formed during the spring. Portmann et al. (1996) argue that this process is as important as denitrification for ozone loss in the Antarctic.

Denitrification involves the sedimentation of large HNO_3-containing particles; however, until recently, it has not been clear exactly what these particles are, or how they form. STS particles are too small (typically radii of $\sim 0.5\,\mu$m) to have sedimentation speeds greater than a metre per day. Similarly, if all background aerosol particles act as nucleation sites for NAT, then NAT particles would also be too small to promote denitrification. The most likely particles to cause denitrification are ice particles. Because of the relatively high amounts of H_2O in the atmosphere, ice particles can grow to the large sizes necessary for efficient sedimentation, and can incorporate gaseous HNO_3 in the form of NAT (e.g. Wofsy et al., 1990). The sedimentation of these ice particles would also result in dehydration of the stratosphere, which inhibits ozone loss, though to a lesser degree than it is promoted by denitrification.

Observations of denitrification have, however, painted a more complicated picture. Analysis of in-situ and remote observations from the Arctic winter of

1994–95 suggested that the denitrification observed was predominantly caused by small number densities of large NAT particles (Waibel et al., 1999). The then-current modelling practice of assuming that all aerosol particles froze to NAT, creating a population of many small NAT particles, led to an underestimation of the true influence of NAT particles on the stratosphere. In addition, satellite-based observations indicated that, during relatively warm winter months in the Antarctic, extensive denitrification can occur without any significant dehydration (Tabazadeh et al., 2000). However, up to this point, no large NAT particles had been measured in-situ.

This changed in the Arctic winter of 1999–2000, during which the most extensive denitrification observed above the Arctic occurred (Popp et al., 2001). In-situ measurements (see Section 2 and Northway et al., 2002) detected HNO_3-containing particles, with diameters as large as 10–20 μm and total number densities in the order of $10^{-4}\,cm^{-3}$ (Fahey et al., 2001). Highly selective nucleation mechanisms, such as low freezing rates of NAT (or NAD) below $\sim$196 K (e.g. Tabazadeh et al., 2001), or NAT formation via ice particles (e.g. Waibel et al., 1999), were put forward to interpret the observations. Because of the length of time needed for these particles to grow, Mann et al. (2003) showed that, regardless of nucleation mechanism, the amount of denitrification likely to occur could be determined using the "closed-flow area" of the vortex. This is based on the degree of concentricity of the vortex and the mass of air with temperatures below T_{NAT} (see Figure 16).

Model studies (Carslaw et al., 2002) have shown that synoptic-scale ice clouds were very unlikely to be the source of the observed "NAT-rocks", and suggested that, although localised gravity waves are known sources of NAT particles (Carslaw et al., 1998a), they would produce only a limited number of the

observed large particles. Fueglistaler et al. (2002) proposed that the gravitational settling of particles from typical Type Ia PSCs, into air supersaturated with respect to NAT, could act as a source for NAT-rocks. However observations of NAT PSCs in situations where this cannot have occurred suggest that this mechanism is not the only source of NAT-rock particles in the stratosphere (Voigt et al., 2005). A number of studies of NAT formation during the winter of 2002/2003 have suggested that observed NAT particle numbers (Larsen et al., 2004; Voigt et al., 2005) and levels of denitrification (Grooß et al., 2005; Davies et al., 2006) can be reproduced using a simple flat nucleation rate of NAT particles, at temperatures below T_{NAT}. The nucleation rates determined are 25×10^{-6} (Larsen et al., 2004), 8×10^{-6} (Voigt et al., 2005), 7.8×10^{-6} (Grooß et al., 2005), and 12×10^{-6} particles $cm^{-3}hr^{-1}$(Davies et al., 2006). Modelling studies of denitrification during previous Arctic winters have determined optimal nucleation rates of a similar magnitude: 2.9×10^{-6} particles $cm^{-3}hr^{-1}$ for the winter 1999/2000 (Mann et al., 2003), and 12×10^{-6} particles $cm^{-3}hr^{-1}$ for the winter 1994/95 (Davies et al., 2005).

5 Summary

To summarise: **(1)** In-situ instrumentation has improved to the point where we can measure the amounts of the major constituents of the condensed phase and their ratios — allowing for the positive identification of STS and NAT particles in the Arctic Stratosphere. **(2)** Satellite instruments can now be used to identify the category of PSCs as well as their synoptic extent - improving the temporal and spatial coverage of observations. **(3)** The major types of PSC particles have been identified, and observed in the stratosphere. Simple ho-

mogeneous nucleation of NAT from STS droplets has been shown to occur at too low a rate to be significant in the stratosphere. Whether NAT nucleates through a classical volume-dependent heterogeneous route, a surface-based pseudo-heterogeneous route, or some other route, is still not clear. **(4)** Our knowledge of the heterogeneous reaction rates for the release of halogens on PSC particles is extensive — but still inadequate for STS droplets, which are the most common PSC type in the Arctic. This lack of knowledge limits the accuracy of the large-scale microphysical models which have recently been developed. **(5)** "NAT-rocks" have been discovered in the Arctic. These large particles have been shown to be important in the denitrification of the stratosphere. **(6)** Global warming at the surface is associated with cooling in the stratosphere. Stratospheric cooling will likely change the frequency of occurrence of PSCs, as well as changing stratospheric chemistry more generally. There is evidence that the volume of Arctic stratosphere susceptible to ozone destruction may be changing, particularly in those years that are generally cold. **(7)** A sufficiently accurate, yet computationally efficient, parameterisation of PSC microphysics and chemistry, for use in global chemistry-climate models, is yet to be developed. This limits the accuracy with which the recovery of the ozone layer, and the impact of stratospheric processes on climate, can be forecast.

References

Baumgardner, D., Dye, J. E., Gandrud, B. W., Knollenburg, R. G., 1992. Interpretation of measurements made by the Foward Scattering Spectrometer Probe (FSSP-300) during the Airbourne Artic Stratosphere Expedition. Journal of Geophysical Research 97 (D8), 8035–8046.

Bertram, A. K., Patterson, D. D., Sloan, J. J., 1996. Mechanisms and temperatures for the freezing of sulfuric acid aerosols measured by FTIR extinction spectroscopy. The Journal of Physical Chemistry 100 (6), 2376–2383.

Bertram, A. K., Sloan, J. J., 1998. The nucleation rate constants and freezing mechanism of nitric acid trihydrate aerosol under stratospheric conditions. Journal of Geophysical Research 103 (D11), 13261–13265.

Beyer, K. D., Seago, S. W., Chang, H. Y., Molina, M. J., 1994. Composition and freezing of aqueous H_2SO_4/HNO_3 solutions under polar stratospheric conditions. Geophysical Research Letters 21 (10), 871–874.

Biermann, U. M., Crowley, J. N., Huthwelker, T., Moortgat, G. K., Crutzen, P. J., Peter, T., 1998. FTIR studies on lifetime prolongation of stratospheric ice particles due to NAT coating. Geophysical Research Letters 25 (21), 3939–3942.

Bogdan, A., Molina, M. J., Kulmala, M., MacKenzie, A. R., Laaksonen, A., 2003. Study of finely divided aqueous systems as an aid to understanding the formation mechanism of polar stratospheric clouds: Case of HNO_3/H_2O and H_2SO_4/H_2O systems. Journal of Geophysical Research 108 (D10), 4302, doi:10.1029/2002JD002605.

Brasseur, G., Solomon, S., 2005. Aeronomy of the Middle Atmosphere, 3rd Edition. Springer, Dordrecht, The Netherlands.

Browell, E. V., Butler, C. F., Ismail, S., Robinette, P. A., Carter, A. F., Hig-

don, N. S., Toon, O. B., Schoeberl, M. R., Tuck, A. F., 1990. Airborne lidar observations in the wintertime Arctic stratosphere: Polar stratospheric clouds. Geophysical Research Letters 17 (4), 385–388.

Carslaw, K. S., Clegg, S. L., Brimblecombe, P., 1995. A thermodynamic model of the system HCL–HNO_3–H_2SO_4–H_2O, including solubilities of HBr, from <200 to 328 K. Journal of Physical Chemistry 99, 11557–11574.

Carslaw, K. S., Kettleborough, J. A., Northway, M. J., Davies, S., Gao, R.-S., Fahey, D. W., Baumgardner, D. G., Chipperfield, M. P., Kleinböhl, A., 2002. A vortex-scale simulation of the growth and sedimentation of large nitric acid hydrate particles. Journal of Geophysical Research 107 (D20), 8300, doi:10.1029/2001JD000467.

Carslaw, K. S., Luo, B. P., Clegg, S. L., Peter, T., Brimblecombe, P., Crutzen, P. J., 1994. Stratospheric aerosol growth and HNO_3 gas phase depletion from coupled HNO_3 and water uptake by liquid particles. Geophysical Research Letters 21 (23), 2479–2482.

Carslaw, K. S., Peter, T., Clegg, S. L., 1997. Modeling the composition of liquid stratospheric aerosols. Reviews of Geophysics 35 (2), 125–154.

Carslaw, K. S., Wirth, M., Tsias, A., Luo, B. P., Dörnbrack, A., Leutbecher, M., Volkert, H., Renger, W., Bacmeister, J. T., Peter, T., 1998a. Particle microphysics and chemistry in remotely observed mountain polar stratospheric clouds. Journal of Geophysical Research 103 (D5), 5785–5796.

Carslaw, K. S., Wirth, M., Tsias, A., Luo, B. P., Dörnbrack, A., Leutbecher, M., Volkert, H., Renger, W., Bacmeister, J. T., Reimer, E., Peter, T., 1998b. Increased stratospheric ozone depletion due to mountain-induced atmospheric waves. Nature 391, 675–678.

Chang, H.-Y. A., Koop, T., Molina, L. T., Molina, M. J., 1999. Phase transitions in emulsified HNO_3/H_2O and $HNO_3/H_2SO_4/H_2O$ solutions. Journal

of Physical Chemistry A 103, 2673–2679.

Cox, R. A., MacKenzie, A. R., Müller, R. H., Peter, T., Crutzen, P. J., 1994. Activation of stratospheric chlorine by reactions in liquid sulphuric acid. Geophysical Research Letters 21 (13), 1439–1442.

Davies, S., Mann, G. W., Carslaw, K. S., Chipperfield, M. P., Kettleborough, J. A., Santee, M. L., Oelhaf, H., Wetzel, G., Sasano, Y., Sugita, T., 2005. 3-D microphysical model studies of Arctic denitrification: comparison with observations. Atmospheric Chemistry and Physics 5, 3093–3109.

Davies, S., Mann, G. W., Carslaw, K. S., Chipperfield, M. P., Remedious, J. J., Allen, G., Waterfall, A. M., Spang, R., Toon, G. C., 2006. Testing our understanding of Arctic denitrification using MIPAS-E satellite measurements in winter 2002/2003. Atmospheric Chemistry and Physics 6, 3149–3161.

Davy, J. G., Somorjai, G. A., 1971. Studies of the vaporization mechanism of ice single crystals. Journal of Chemical Physics 55, 3624–3636.

Disselkamp, R. S., Anthony, S. E., Prenni, A. J., Onasch, T. B., Tolbert, M. A., 1996. Crystallization kinetics of nitric acid dihydrate aerosols. Journal of Physical Chemistry 100, 9127–9137.

Donaldson, D. J., Anderson, D., 1999. Does molecular HNO_3 adsorb onto sulfuric acid droplet surfaces? Geophysical Research Letters 26 (24), 3625–3628.

Drdla, K., 2007 Re-examining polar ozone loss: Do polar stratospheric clouds really control chlorine activation? manuscript in preparation.

Drdla, K., Gandrud, B. W., Baumgardner, D., Wilson, J. C., Bui, T. P., Hurst, D., Schauffler, S. M., Jost, H., Greenblatt, J. B., Webster, C. R., 2003. Evidence for the widespread presence of liquid-phase particles during the 1999–2000 Arctic winter. Journal of Geophysical Research, 107, 8318,

doi:10.1029/2001JD001127, 2002. [printed 108 (D5), 2003]

Drdla, K., Schoeberl, M. R., 2003. Microphysical modelling of the 1999–2000 artic winter: 2. chlorine activation and ozone depletion. Journal of Geophysical Research, 107, 8319, doi:10.1029/2001JD001159, 2002. [printed 108 (D5), 2003]

Drdla, K., Turco, R. P., 1991. Denitrification through PSC formation: A 1-D model incorporating temperature oscillations. Journal of Atmospheric Chemistry 12, 319–366.

Duft, D., Leisner, T., 2004. Laboratory evidence for volume-dominated nucleation of ice in supercooled water microdroplets. Atmospheric Chemistry and Physics 4, 1997–2000.

Dye, J. E., Baumgardner, D., Gandrud, B. W., Kawa, S. R., Kelly, K. K., Loewenstein, M., Ferry, G. V., Chan, K. R., Gary, B. L., 1992. Particle size distributions in Arctic polar stratospheric clouds, growth and freezing of sulfuric acid droplets and implications for cloud formation. Journal of Geophysical Research 97 (D8), 8012–8034.

Elrod, M. J., Koch, R. E., Kim, J. E., Molina, M. J., 1995. HCl vapour pressures and reaction probabilities for $ClONO_2$ + HCl on liquid H_2SO_4–HNO_3–HCl–H_2O solutions. Faraday Discussions 100, 269–278.

Eyring, V., Harris, N. R. P., Rex, M., Shepherd, T. G., Fahey, D. W., Amanatidis, G. T., Austin, J., Chipperfield, M. P., Dameris, M., Forster, P. M. D. F., Gettelman, A., Graf, H. F., Nagashima, T., Newman, P. A., Pawson, S., Prather, M. J., Pyle, J. A., Salawitch, R. J., Santer, B. D., , Waugh, D. W., 2005. A strategy for process-oriented validation of coupled chemistry-climate models. Bulletin Of The American Meteorological Society 86 (8), 1117–1133.

Fahey, D. W., Gao, R. S., Carslaw, K. S., Kettleborough, J., Popp, P. J.,

Northway, M. J., Holecek, J. C., Ciciora, S. C., McLaughlin, R. J., Thompson, T. L., Winkler, R. H., Baumgardner, D. G., Gandrud, B., Wennberg, P. O., Dhaniyala, S., McKinney, K., Peter, T., Salawitch, R. J., Bui, T. P., Elkins, J. W., Webster, C. R., Atlas, E. L., Jost, H., Wilson, J. C., Herman, R. L., Kleinböhl, A., von König, M., 2001. The detection of large HNO_3-containing particles in the winter Arctic stratosphere. Science 291, 1026–1031.

Fahey, D. W., Kelly, K. K., Ferry, G. V., Poole, L. R., Wilson, J. C., Murray, D. M., Loewenstein, M., Chan, K. R., 1989. In situ measurements of total reactive nitrogen, total water, and aerosol in a polar stratospheric cloud in the Antarctic. Journal of Geophysical Research 94 (D9), 11299–11315.

Fahey, D. W., Kelly, K. K., Kawa, S. R., Tuck, A. F., Loewenstein, M., Chan, K. R., 1990. Observations of denitrification and dehydration in the winter polar stratospheres. Nature 344, 321–324.

Farman, J. C., Gardiner, B. G., Shanklin, J. D., 1985. Large losses of total ozone in Antartica reveal seasonal ClOx/NOx interaction. Nature 315, 207–210.

Fortin, T. J., Drdla, K., Iraci, L. T., Tolbert, M. A., 2003. Ice condensation on sulfuric acid tetrahydrate: Implications for polar stratospheric ice clouds. Atmospheric Chemistry and Physics 3 (4), 987–997.

Fromm, M., Alfred, J., Pitts, M., 2003. A unified, long-term, high-latitude stratospheric aerosol and cloud database using SAM II, SAGE II, and POAM II/III data: Algorithm description, database definition, and climatology. Journal of Geophysical Research 108 (D12), 4366, doi:10.1029/2002JD002772.

Fueglistaler, S., Luo, B. P., Voigt, C., Carslaw, K. S., Peter, T., 2002. NAT-rock formation by mother clouds: a microphysical model study. Atmospheric

Chemistry and Physics 2 (2), 93–98.

Gable, C. M., Betz, H. F., Maron, S. H., 1950. Phase equilibria of the system sulfer trioxide-water. American Chemical Society Journal 72, 1445–1448.

Geer, A. J., Lahoz, W. A., Bekki, S., Bormann, N., Errera, Q., Eskes, H. J., Fonteyn, D., Jackson, D. R., Juckes, M. N., Massart, S., Peuch, V.-H., Rharmili, S., Segers, A., 2006. The ASSET intercomparison of ozone analyses: method and first results. Atmospheric Chemistry and Physics 6, 5445–5474.

Gierens, K., 2003. On the transition between heterogeneous and homogeneous freezing. Atmospheric Chemistry and Physics 3 (2), 437–446.

Gobbi, G. P., Di Donfrancesco, G., Adriani, A., 1998. Physical properties of stratospheric clouds during the Antarctic winter of 1995. Journal of Geophysical Research 103 (D9), 10859–10873.

Grooß, J.-U., Günther, G., Müller, R., Konopka, P., Bausch, S., Schlager, H., Voigt, C., Volk, C. M., Toon, G. C., 2005. Simulation of denitrification and ozone loss for the Arctic winter 2002/2003. Atmospheric Chemistry and Physics 5, 1437–1448.

Hamill, P., Turco, R. P., Toon, O. B., 1988. On the growth of nitric and sulfuric acid aerosol particles under stratospheric conditions. Journal of Atmospheric Chemistry 7, 287–315.

Hanson, D., Mauersberger, K., 1988. Laboratory studies of the nitric acid trihydrate: Implications for the south polar stratosphere. Geophysical Research Letters 15 (8), 855–858.

Hanson, D. R., 1990. The vapor pressures of supercooled HNO_3/H_2O solutions. Geophysical Research Letters 17 (4), 421–423.

Hanson, D. R., 1998. Reaction of $ClONO_2$ with H_2O and HCL in sulfuric acid and $HNO_3/H_2SO_4/H_2O$ mixtures. Journal of Physical Chemistry A 102,

4794–4807.

Hinds, W. C., 1999. Aerosol Technology, 2nd. edition, pp. 482, Wiley, New York.

Hofmann, D. J., 1990. Stratospheric cloud micro-layers and small-scale temperature variations in the Artic in 1989. Geophysical Research Letters 17 (4), 369–372.

Hofmann, D. J., Deshler, T., 1990. Balloonborne measurements of polar stratospheric clouds and ozone at -93 ℃ in the Arctic in February 1990. Geophysical Research Letters 17 (12), 2185–2188.

Hofmann, D. J., Deshler, T., Arnold, F., Schlager, H., 1990. Balloon observations of nitric acid aerosol formation in the Arctic stratosphere: II. aerosol. Geophysical Research Letters 17 (9), 1279–1282.

Höpfner, M., Luo, B. P., Massoli, P., Cairo, F., Spang, R., Snels, M., Donfrancesco, G. D., Stiller, G., von Clarmann, T., Fischer, H., Biermann, U., 2006. Spectroscopic evidence for NAT, STS, and ice in MIPAS infrared limb emission measurements of polar stratospheric clouds. Atmospheric Chemistry and Physics 6, 1201–1219.

Huthwelker, T., Peter, T., Luo, B. P., Clegg, S. L., Carslaw, K. S., Brimblecombe, P., 1995. Solubility of HOCl in water and aqueous H_2SO_4 to stratospheric conditions. Journal of Atmospheric Chemistry 21, 81–95.

Iraci, L. T., Fortin, T. J., Tolbert, M. A., 1998. Dissolution of sulfuric acid tetrahydrate at low temperatures and subsequent growth of nitric acid trihydrate. Journal of Geophysical Research 103 (D7), 8491–8498.

Iraci, L. T., Middlebrook, A. M., Tolbert, M. A., 1995. Laboratory studies of the formation of polar stratospheric clouds — nitric-acid condensation on thin sulfuric-acid films. Journal of Geophysical Research 100 (D10), 20969–20977.

Jaenicke, R., 1998. Atmospheric Aerosol Size Distribution, in Atmospheric Particles, R. M. Harrison and R. van Griecken (eds.), ch. 1, Wiley, New York.

Kim, Y., Choi, W., Lee, K. M., Park, J. H., Massie, S. T., Sasano, Y., Nakajima, H., Yokota, T., 2006. Polar stratospheric clouds observed by the ILAS-II in the Antarctic region: Dual compositions and variation of compositions during June to August of 2003. Journal of Geophysical Research 111, D13S90, doi:10.1029/2005JD006445.

Knopf, D. A., Koop, T., Luo, B. P., Weers, U. G., Peter, T., 2002. Homogeneous nucleation of NAD and NAT in liquid stratospheric aerosols: Insufficient to explain denitrification. Atmospheric Chemistry and Physics 2 (3), 207–214.

Koop, T., Biermann, U. M., Raber, W., Luo, B. P., Crutzen, P. J., Peter, T., 1995. Do stratospheric aerosol droplets freeze above the ice frost point? Geophysical Research Letters 22 (8), 917–920.

Koop, T., Carslaw, K. S., 1996. Melting of $H_2SO_4/4H_2O$ particles upon cooling: Implications for polar stratospheric clouds. Science 272, 1638–1641.

Koop, T., Carslaw, K. S., Peter, T., 1997a. Thermodynamic stability and phase transitions of PSC particles. Geophysical Research Letters 24 (17), 2199–2202.

Koop, T., Luo, B., Tsias, A., Peter, T., 2000. Water activity as the determinant for homogeneous ice nucleation in aqueous solutions. Nature 406, 611–614.

Koop, T., Luo, B. P., Biermann, U. M., Crutzen, P. J., Peter, T., 1997b. Freezing of $HNO_3/H_2SO_4/H_2O$ solutions at stratospheric temperatures: Nucleation statistics and experiments. The Journal of Physical Chemistry A 101, 1117–1133.

Koop, T., Ng, H. P., Molina, L. T., Molina, M. J., 1998. A new optical tech-

nique to study aerosol phase transitions: The nucleation of ice from H_2SO_4 aerosols. Journal of Physical Chemistry A 102, 8924–8931.

Kühl, S., Dörnbrack, A., Wilms-Grabe, W., Sinnhuber, B.-M., Platt, U., Wagner, T., 2004. Observational evidence of rapid chlorine activation by mountain waves above northern Scandinavia. Journal of Geophysical Research 109, D22309, doi:10.1029/2004JD004797.

Larsen, N., Knudsen, B. M., Svendsen, S. H., Deshler, T., Rosen, J. M., Kivi, R., Weisser, C., Schreiner, J., Mauerberger, K., Cairo, F., Ovarlez, J., Oelhaf, H., Spang, R., 2004. Formation of solid particles in synoptic-scale Arctic PSCs in early winter 2002/2003. Atmospheric Chemistry and Physics 4 (7), 2001–2013.

Lee, K. M., Park, J. H., Kim, Y., Choi, W., Cho, H. K., Massie, S. T., Sasano, Y., Yokota, T., 2003. Properties of polar stratospheric clouds observed by ILAS in early 1997. Journal of Geophysical Research 108 (D7), 4228, doi:10.1029/2002JD002854.

Liu, L., Mishchenko, M. I., 2001. Constraints on PSC particle microphysics derived from lidar observations. Journal of Quantitative Spectroscopy & Radiative Transfer 70, 817–831.

Lowe, D., 2003. Design and implementation of a multi-component, non-equilibrium model for the study of polar stratospheric clouds. Lancaster University, PhD Thesis.

Lowe, D., MacKenzie, A. R., Nikiforakis, N., Kettleborough, J., 2003. A condensation-mass advection based model for the simulation of liquid polar stratospheric clouds. Atmospheric Chemistry and Physics 3, 29–38.

Lowe, D., MacKenzie, A. R., Schlager, H., Voigt, C., Dörnbrack, A., Mahoney, M. J., Cairo, F., 2006. Liquid particle composition and heterogeneous reactions in a mountain wave polar stratospheric cloud. Atmospheric Chemistry

and Physics 6 (11), 3611–3623.

Luo, B. P., Voigt, C., Fueglistaler, S., Peter, T., 2003. Extreme NAT supersaturations in mountain wave ice PSCs — a clue to NAT formation. Journal of Geophysical Research 108 (D15), 4441, doi:10.1029/2002JD003104.

MacKenzie, A. R., 2003. Handbook of Atmospheric Science. C. N. Hewitt and A. Jackson (eds.), Blackwell, Oxford, UK, Ch. 7, pp. 188–210.

MacKenzie, A. R., Kulmala, M., Laaksonen, A., Vesala, T., 1995. On the theories of type 1 polar stratospheric cloud formation. Journal of Geophysical Research 100 (D6), 11275–11289.

MacKenzie, A. R., Kulmala, M., Laaksonen, A., Vesala, T., 1997. Correction to "On the theories of type 1 polar stratospheric cloud formation" by A. R. MacKenzie, et al. Journal Of Geophysical Research 102 (D16), 19729–10730.

MacKenzie, A. R., Laaksonen, A., Batris, E., Kulmala, M., 1998. The Turnbull correlation and the freezing of stratospheric areosol droplets. Journal of Geophysical Research 103 (D9), 10875–10884.

Mann, G. W., Davies, S., Carslaw, K. S., Chipperfield, M. P., 2003. Factors controlling Artic denitrification in cold winters of the 1990s. Atmospheric Chemistry and Physics 3 (2), 403–416.

Marti, J., Mauersberger, K., 1993. A survey and new measurements of ice vapor pressure at temperatures between 170 and 250 K. Geophysical Research Letters 20 (5), 363–366.

Maturilli, M., Neuber, R., Massoli, P., Cairo, F., Adriani, A., Moriconi, M. L., Donfrancesco, G. D., 2005. Differences in Arctic and Antarctic PSC occurence as observed by lidar in Ny-ålesund (79°N, 12°E) and McMurdo (78°S, 167°E). Atmospheric Chemistry and Physics 5, 2081–2090.

McCormick, M. P., Chu, W. P., Grams, G. W., Hamill, P., Herman, B. M., McMaster, L. R., Pepin, T. J., Russell, P. B., Steele, H. M., Swissler, T. J.,

1981. High-latitude stratospheric aerosols measured by the SAM-II satellite system in 1978 and 1979. Science 214 (4518), 328–331.

McCormick, M. P., Steele, H. M., Hamill, P., Chu, W. P., Swissler, T. J., 1982. Polar stratospheric cloud sightings by SAM II. Journal of the Atmospheric Sciences 39 (6), 1387–1397.

Meilinger, S. K., Koop, T., Luo, B. P., Huthwelker, T., Carslaw, K. S., Krieger, U., Crutzen, P. J., Peter, T., 1995. Size-dependent stratospheric droplet composition in lee wave temperature fluctuations and their potential role in PSC freezing. Geophysical Research Letters 22 (22), 3031–3034.

Middlebrook, A. M., Iraci, L. T., McNeill, L. S., Koehler, B. G., Wilson, M. A., Saastad, O. W., Tolbert, M. A., Hanson, D. R., 1993. Fourier transform-infrared studies of thin H_2SO_4/H_2O films: Formation, water uptake, and solid-liquid phase changes. Journal of Geophysical Research 98 (D11), 20473–20481.

Middlebrook, A. M., Tolbert, M. A., Drdla, K., 1996. Evaporation studies of model polar stratospheric cloud films. Geophysical Research Letters 23 (16), 2145–2148.

Möhler, O., Bunz, H., Stetzer, O., 2006. Homogeneous nucleation rates of nitric acid dihydrate (nad) at simulated stratospheric conditions - part II: Modelling. Atmospheric Chemistry And Physics 6 (10), 3035–3047.

Molina, M. J., Zhang, R., Wooldridge, P. J., McMahon, J. R., Kim, J. E., Chang, H. Y., Beyer, K. D., 1993. Physical chemistry of the $H_2SO_4/HNO_3/H_2O$ system: Implications for polar stratospheric clouds. Science 261, 1418–1423.

Natsheh, A. A., Nadykto, A. B., Mikkelsen, K. V., Yu, F., Ruuskanen, J., 2006. Coexistance of metastable nitric acid dihydrates: A molecular level contribution to understanding the formation of polar stratospheric clouds

crystals. Chemical Physics Letters 426, 20–25.

Northway, M. J., Gao, R. S., Popp, P. J., Holecek, J. C., Fahey, D. W., Carslaw, K. S., Tolbert, M. A., Lait, L. R., Dhaniyala, S., Flagan, R. C., Wennberg, P. O., Mahoney, M. J., Herman, R. L., Toon, G. C., Bui, T. P., 2002. An analysis of large HNO_3-containing particles sampled in the Arctic stratosphere during the winter of 1999/2000. Journal of Geophysical Research 107 (D20), 8298, doi:10.1029/2001JD001079.

Pawson, S., Naujokat, B., 1999. The cold winters of the middle 1990s in the northern lower stratosphere. Journal of Geophysical Research 104 (D12), 14,209–14,222.

Peter, T., Brühl, C., Crutzen, P. J., 1991. Increase in the PSC-formation probability caused by high-flying aircraft. Geophysical Research Letters 18 (8), 1465–1468.

Peter, T., Müller, R., Crutzen, P. J., Deshler, T., 1994. The lifetime of leewave-induced ice particles in the Artic stratosphere: II. stabilization due to NAT-coating. Geophysical Research Letters 21 (13), 1331–1334.

Peter, T., 1996. Airborne particle analysis for climate studies. Science, 273, 1352–1353.

Peter, T., 1997. Microphysics and heterogeneous chemistry of polar stratospheric clouds. Annual Reviews of Physical Chemistry 48, 785–822.

Poole, L., Trepte, C., Harvey, V., Toon, G., VanValkenburg, R. L., 2003. SAGE III observations of Arctic polar stratospheric clouds — December 2002. Geophysical Research Letters 30 (23), 2216, doi:10.1029/2003GL018496.

Poole, L. R., McCormick, M. P., 1988. Airborne lidar observations of arctic polar stratospheric clouds: Indications of two distinct growth stages. Geophysical Research Letters 15 (1), 21–23.

Poole, L. R., Pitts, M. C., 1994. Polar stratospheric cloud climatology based

on Stratospheric Aerosol Measurement II observations from 1978 to 1989. Journal of Geophysical Research 99 (D6), 13083–13089.

Popp, P. J., Northway, M. J., Holecek, J. C., Gao, R. S., Fahey, D. W., Elkins, J. W., Hurst, D. F., Romashkin, P. A., Toon, G. C., Sen, B., Schauffler, S. M., Salawitch, R. J., Webster, C. R., Herman, R. L., Jost, H., Bui, T. P., Newman, P. A., Lait, L. R., 2001. Severe and extensive denitrification in the 1999–2000 Arctic winter stratosphere. Geophysical Research Letters 28 (15), 2875–2878.

Portmann, R. W., Solomon, S., Garcia, R. R., Thomason, L. W., Poole, L. R., McCormick, M. P., 1996. Role of aerosol variations in anthropogenic ozone depletion in the polar regions. Journal of Geophysical Research 101 (D17), 229991–23006.

Ravishankara, A. R., (ed.) 2003. Atmospheric chemistry: Long-term issues. Chemical Reviews 103 (12).

Reichardt, J., Reichardt, S., Yang, P., McGee, T. J., 2002. Retrieval of polar stratospheric cloud microphysical properties from lidar measurements: Dependence on particle shape assumptions. Journal of Geophysical Research 107 (D20), 8282, doi:10.1029/2001JD001021.

Rex, M., Salawitch, R. J., von der Gathen, P., Harris, N. R. P., Chipperfield, M. P., Naujokat, B., 2004. Arctic ozone loss and climate change. Geophysical Research Letters 31, L04116, doi:10.1029/2003GL018844.

Rosen, J. M., 1971. The boiling point of stratospheric aerosols. Journal of Applied Meteorology 10, 1044–1046.

Rosen, J. M., Oltmans, S. J., Evans, W. F., 1989. Balloon borne observations of PSCs, frost point, ozone and nitric acid in the North polar vortex. Geophysical Research Letters 16 (8), 791–794.

SAGE III ATBD Team, 2002. SAGE III Algorithm Theoretical Basis Docu-

ment (ATBD) Transmission Level 1B Products. NASA, 2nd Edition.

Salcedo, D., Molina, L. T., Molina, M. J., 2000. Nucleation rates of nitric acid dihydrate in 1:2 HNO_3/H_2O solutions at stratospheric temperatures. Geophysical Research Letters 27 (2), 193–196.

Salcedo, D., Molina, L. T., Molina, M. J., 2001. Homogeneous freezing of concentrated aqueous nitric acid solutions at polar stratospheric temperatures. Journal of Physical Chemistry A 105, 1433–1439.

Sander, S. P., Friedl, R. R., Ravishankara, A. R., Golden, D. M., Kolb, C. E., Kurylo, M. J., Molina, M. J., Moortgat, G. K., Keller-Rudek, H., Finlayson-Pitts, B. J., Wine, P. H., Huie, R. E., Orkin, V. L., 2006. Chemical kinetics and photochemical data for use in atmospheric studies. Evaluation number 15, JPL Publication 06-02, Pasadena.

Santacesaria, V., Stefanutti, L., MacKenzie, A. R., Guzzi, D., 2001. Polar stratospheric cloud climatology (1989–1997) from LIDAR measurements over Dumont d'Urville (Antarctica). Tellus B 53, 306–321.

Schlager, H., Arnold, F., Hofmann, D., Deshler, T., 1990. Balloon observations of nitric acid aerosol formation in the Artic stratosphere: I. gaseous nitric acid. Geophysical Research Letters 17 (9), 1275–1278.

Schreiner, J., Voigt, C., Weisser, C., Kohlmann, A., Mauersberger, K., Deshler, T., Kröger, C., Kjome, N., Larsen, N., Adriani, A., Cairo, F., Donfrancesco, G. D., Ovarlez, J., Ovarlez, H., Dörnbrack, A., 2003. Chemical, microphysical, and optical properties of polar stratospheric clouds. Journal of Geophysical Research 107, 8313, doi:10.1029/2001JD000825, 2002.[printed 108 (D5), 2003].

Schreiner, J., Voigt, C., Zink, P., Kohlmann, A., Knopf, D., Weisser, C., Budz, P., Mauersberger, K., 2002. A mass spectrometer system for analysis of polar

stratospheric aerosols. Review of Scientific Instruments 73 (2), 446–452.

Schreiner, J., Voigt, C., Kohlmann, A., Arnold, F., Mauersberger, K., Larsen, N., 1999. Chemical analysis of polar stratospheric cloud particles. Science 283, 968–970.

Seinfeld, J. H., Pandis, S. N., 2006. Atmospheric Chemistry and Physics, 2nd Edition. Wiley, New York.

Sheridan, P. J., Brrok, C. A., Wilson, J. C., 1994. Aerosol particles in the upper troposphere and lower stratosphere: Elemental composition and morphology of individual particles in northern midlatitudes. Geophysical Research Letters 21 (23), 2587–2590.

Shi, Q., Jayne, J. T., Kolb, C. E., Worsnop, D. R., Davidovits, P., 2001. Kinetic model for reaction of $ClONO_2$ with H_2O and HCL and HOCl with HCL in sulfuric acid solutions. Journal of Geophysical Research 106 (D20), 24259–24274.

Shibata, T., Iwasaka, Y., Fujiwara, M., Hayashi, M., Nagatani, M., Shiraishi, K., Adachi, H., Sakai, T., Susumu, K., Nakura, Y., 1997. Polar stratospheric clouds observed by lidar over spitsbergen in the winter of 1994/1995: Liquid particles and vertical "sandwich" structure. Journal of Geophysical Research 102 (D9), 10829–10840.

Solomon, S., Garcia, R. R., Rowland, F. S., Wuebbles, D. J., 1986. On the depletion of Antartic ozone. Nature 321, 755–758.

Solomon, S., 1990. Progress towards a quantitative understanding of Antarctic ozone depletion. Nature 347, 347–354.

Solomon S, 1999. Stratospheric ozone depletion: A review of concepts and history Reviews of Geophysics 37 (3): 275-316.

Solomon S, 2004. The hole truth - What's news (and what's not) about the

ozone hole. Nature 427, 289-291

Spang, R., Remedios, J. J., 2003. Observations of a distinctive infra-red spectral feature in the atmospheric spectra of polar stratospheric clouds measured by the CRISTA instrument. Geophysical Research Letters 30 (16), 1875, doi:10.1029/2003GL017231.

Spang, R., Remedios, J. J., Kramer, L. J., Poole, L. R., Fromm, M. D., Müller, M., Baumgarten, G., Konopka, P., 2005. Polar stratospheric cloud observations by MIPAS on ENVISAT: detection method, validation and analysis of the northern hemisphere winter 2002/2003. Atmospheric Chemistry and Physics 5 (3), 679–692.

Spang, R., Riese, M., Offermann, D., 2001. CRISTA-2 observations of the south polar vortex in winter 1997: A new dataset for polar process studies. Geophysical Research Letters 28 (16), 3159–3162.

Stanford, J. L., Davis, J. S., 1974. A century of stratospheric cloud reports: 1870–1972. Bulletin of the American Meteorological Society 55, 213–219.

Steele, H. M., Hamill, P., 1981. Effects of temperature and humidity on the growth and optical properties of sulfuric acid-water droplets in the stratosphere. Journal of Aerosol Science 12, 517–528.

Stefanutti, L., MacKenzie, A. R., Balestri, S., Khattatov, V., Fiocco, G., Kyrö, E., Peter, T., 1999. Airborne Polar Experiment-Polar Ozone, Leewaves, Chemistry, and Transport (APE-POLECAT): Rationale, road map, and summary of measurements. Journal of Geophysical Research 104 (D19), 23941–23959.

Stetzer, O., Möhler, O., Wagner, R., Benz, S., Saathoff, H., Bunz, H., Indris, O., 2006. Homogeneous nucleation rates of nitric acid dihydrate (NAD) at simulated stratospheric conditions — part I: Experimental results. Atmo-

spheric Chemistry and Physics 6, 3023–3033.

Strawa, A. W., Drdla, K., Fromm, M., Pueschel, R. F., Hoppel, K. W., Browell, E. V., Hamill, P., Dempsey, D. P., 2002. Discriminating types Ia and Ib polar stratospheric clouds in POAM satellite data. Journal of Geophysical Research 107 (D20), 8291, doi:10.1029/2001JD000458.

Tabazadeh, A., Djikaev, Y. S., Hamill, P., Reiss, H., 2002a. Laboratory evidence for surface nucleation of solid polar stratospheric cloud particles. The Journal of Physical Chemistry A 106, 10238–10246.

Tabazadeh, A., Djikaev, Y. S., Reiss, H., 2002b. Surface crystallization of supercooled water in clouds. Proceedings of the National Academy of Sciences of the United States of America 99 (25), 15873–15878.

Tabazadeh, A., Jensen, E. J., Toon, O. B., Drdla, K., Schoeberl, M. R., 2001. Role of the stratospheric polar freezing belt in denitrification. Science 291, 2591–2594.

Tabazadeh, A., Santee, M. L., Danilin, M. Y., Pumphrey, H. C., Newman, P. A., Hamill, P. J., Mergenthaler, J. L., 2000. Quantifying denitrification and its effect on ozone recovery. Science 288, 1407–1411.

Tabazadeh, A., Toon, O. B., Hamill, P., 1995. Freezing behavior of stratospheric sulfate aerosols inferred from trajectory studies. Geophysical Research Letters 22 (13), 1725–1728.

Tabazadeh, A., Turco, R. P., Drdla, K., Jacobson, M. Z., 1994. A study of type I polar stratospheric cloud formation. Geophysical Research Letters 21 (15), 1619–1622.

Thomason, L. W., Poole, L. R., Deshler, T., 1997. A global climatology of stratospheric aerosol surface area density deduced from Stratospheric Aerosol and Gas Experiment II measurements: 1984–1994. Journal of Geo-

physical Research 102 (D7), 8967–8976.

Tolbert, M. A., Toon, O. B., 2001. Solving the PSC mystery. Science 292, 61–63.

Toohey, D. W., Availone, L. M., Lait, L. R., Newman, P. A., Schoeberl, M. R., Fahey, D. W., Woodbridge, E. L., Anderson, J. G., 1993. The seasonal evolution of reactive chlorine in the northern hemisphere stratosphere. Science 261, 1134–1136.

Toon, O. B., Browell, E. V., Kinne, S., Jordan, J., 1990. An analysis of lidar observations of polar stratospheric clouds. Geophysical Research Letters 17 (4), 393–396.

Toon, O. B., Hamill, P., Turco, R. P., Pinto, J., 1986. Condensation of HNO_3 and HCL in the winter polar stratospheres. Geophysical Research Letters 13 (12), 1284–1287.

Toon, O. B., Tabazadeh, A., Browell, E. V., 2000. Analysis of lidar observations of Arctic polar stratospheric clouds during January 1989. Journal of Geophysical Research 105 (D16), 20589–20615.

Tsias, A., Prenni, A. J., Carslaw, K. S., Onasch, T. P., Luo, B. P., Tolbert, M. A., Peter, T., 1997. Freezing of polar stratospheric clouds in orographically induced strong warming events. Geophysical Research Letters 24 (18), 2303-2306, 10.1029/97GL02181.

Tsias, A., Wirth, M., Carslaw, K. S., Biele, J., Mehrtens, H., Reichardt, J., Wedekind, C., Weiß, V., Renger, W., Neuber, R., von Zahn, U., Stein, B., Santacesaria, V., Stefanutti, L., Fierli, F., Bacmeister, J., Peter, T., 1999. Aircraft lidar observation of an enchanced type Ia polar stratospheric clouds during APE-POLECAT. Journal of Geophysical Research 104 (D19), 23961–23969.

Turco, R. P., Toon, O. B., Hamill, P., 1989. Heterogeneous physiochemistry

of the polar ozone hole. Journal of Geophysical Research 94 (D14), 16493–16510.

Vincent, J. H., 2007. Aerosol Sampling, 2nd edition, Wiley, New York.

Voigt, C., Schlager, H., Luo, B. P., Dörnbrack, A., Roiger, A., Stock, P., Curtius, J., Vössing, H., Borrmann, S., Davies, S., Konopka, P., Schiller, C., Shur, G., Peter, T., 2005. Nitric acid trihydrate (NAT) formation at low NAT supersaturations in polar stratospheric clouds (PSCs). Atmospheric Chemistry and Physics 5 (5), 1371–1380.

Voigt, C., Schreiner, J., Kohlmann, A., Zink, P., Mauersberger, K., Larsen, N., Deshler, T., Kröger, C., Rosen, J., Adriani, A., Cairo, F., Donfrancesco, G. D., Viterbini, M., Ovarlez, J., Ovarlez, H., David, C., Dörnbrack, A., 2000a. Nitric acid trihydrate (NAT) in polar stratospheric clouds. Science 290, 1756–1758.

Voigt, C., Tsias, A., Dörnbrack, A., Meilinger, S., Luo, B., Schreiner, J., Larsen, N., Mauersberger, K., Peter, T., 2000b. Non-equilibrium compositions of liquid polar stratospheric clouds in gravity waves. Geophysical Research Letters 27 (23), 3873–3876.

von König, M., Bremer, H., Kleinböhl, A., Küllmann, H., Künzi, K. F., Goede, A. P. H., Browell, E. V., Grant, W. B., Burris, J. F., McGee, T. J., Twigg, L., 2002. Using gas-phase nitric acid as an indicator of PSC composition. Journal of Geophysical Research 107 (D20), doi:10.1029/2001JD001041.

Vrbka, L., Jungwirth, P., 2006. Homogeneous freezing of water starts in the subsurface. The Journal of Physical Chemistry B 110, 18126–18129.

Waibel, A. E., Peter, T., Carslaw, K. S., Oelhaf, H., Wetzel, G., Crutzen, P. J., Pöschl, U., Tsias, A., Reimer, E., Fischer, H., 1999. Artic ozone loss due to denitrification. Science 283, 2064–2069.

Waugh, D. W., Randel, W. J., 1999. Climatology of Arctic and Antarctic polar

vortices using elliptical diagnostics. Journal of the Atmospheric Sciences 56 (11), 1594–1613.

Webster, C. R., May, R. D., Toohey, D. W., Avallone, L. M., Anderson, J. G., Newman, P., Lait, L., Schoeberl, M. R., Elkins, J. W., Chan, K. R., 1993. Chlorine chemistry on polar stratospheric cloud particles in the arctic winter. Science 261, 1130–1136.

Wirth, M., Tsias, A., Dörnbrack, A., Weiß, V., Carslaw, K. S., Leutbecher, M., Renger, W., Volkert, H., Peter, T., 1999. Model-guided lagrangian observation and simulation of mountain polar stratospheric clouds. Journal Of Geophysical Research 104 (D19), 23971–23981.

WMO, 2006. Scientific assessment of ozone depletion: 2006. Report 50, Global Ozone Research and Monitoring Project, Geneva.

Wofsy, S. C., Salawitch, R. J., Yatteau, J. H., McElroy, M. B., Gandrud, B. W., Dye, J. E., Baumgardner, D., 1990. Condensation of HNO_3 on falling ice particles: Mechanism for denitrification in the polar stratosphere. Geophysical Research Letters 17 (4), 449–452.

Worsnop, D. R., Fox, L. E., Zahniser, M. S., Wofsy, S. C., 1993. Vapor-pressures of solid hydrates of nitric-acid — implications for polar stratospheric clouds. Science 259 (5091), 71–74.

Yang, H. S., Finlayson-Pitts, B. J., 2001. Infrared spectroscopic studies of binary solutions of nitric acid and water and ternary solutions of nitric acid, sulfuric acid, and water at room temperature: Evidence for molecular nitric acid at the surface. Journal of Physical Chemistry A 105 (10), 1890–1896.

Zhang, R., Jayne, J. T., Molina, M. J., 1994a. Heterogeneous interactions of $ClONO_2$ and HCl with sulfuric acid tetrahydrate: Implications for the stratosphere. Journal of Physical Chemistry 98 (3), 867–874.

Zhang, R., Leu, M.-T., Keyser, L. F., 1994b. Heterogeneous reactions of

$ClONO_2$, HCl, and HOCl on liquid sulfuric acid surfaces. Journal of Physical Chemistry 98, 13563–13574.

Zhang, R., Leu, M.-T., Keyser, L. F., 1995. Hydrolysis of N_2O_5 and $ClONO_2$ on the $H_2SO_4/HNO_3/H_2O$ ternary solutions under stratospheric conditions. Geophysical Research Letters 22 (12), 1493–1496.

Zhang, R., Wooldridge, P. J., Molina, M. J., 1993. Vapor pressure measurements for the $H_2SO_4/HNO_3/H_2O$ and $H_2SO_4/HCl/H_2O$ systems: Incorporation of stratospheric acids into background sulfate aerosols. Journal of Physical Chemistry 97, 8541–8548.

Zhang, R. Y., Leu, M. T., Molina, M. J., 1996. Formation of polar stratospheric clouds on preactivated background aerosols. Geophysical Research Letters 23 (13), 1669–1672.

Zondlo, M. A., Hudson, P. K., Prenni, A. J., Tolbert, M. A., 2000. Chemistry and microphysics of polar stratospheric clouds and cirrus clouds. Annual Review of Physical Chemistry 51, 473–499.

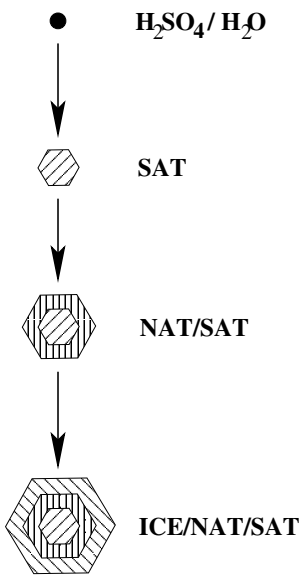

Fig. 1. The 3-stage model of PSC development.

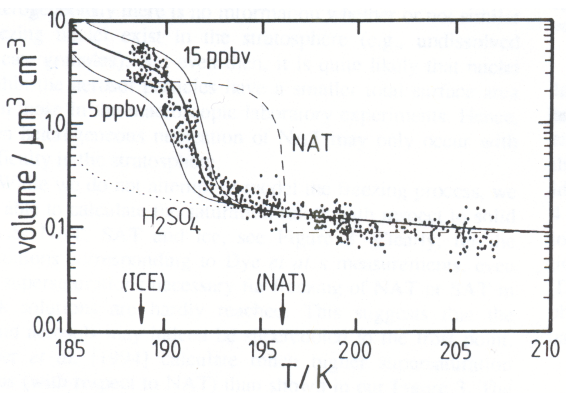

Fig. 2. Particle volumes of Dye et al. (1992) compared with model calculations. From Carslaw et al. (1994).Copyright 1994 American Geophysical Union. Reproduced by permission of American Geophysical Union.

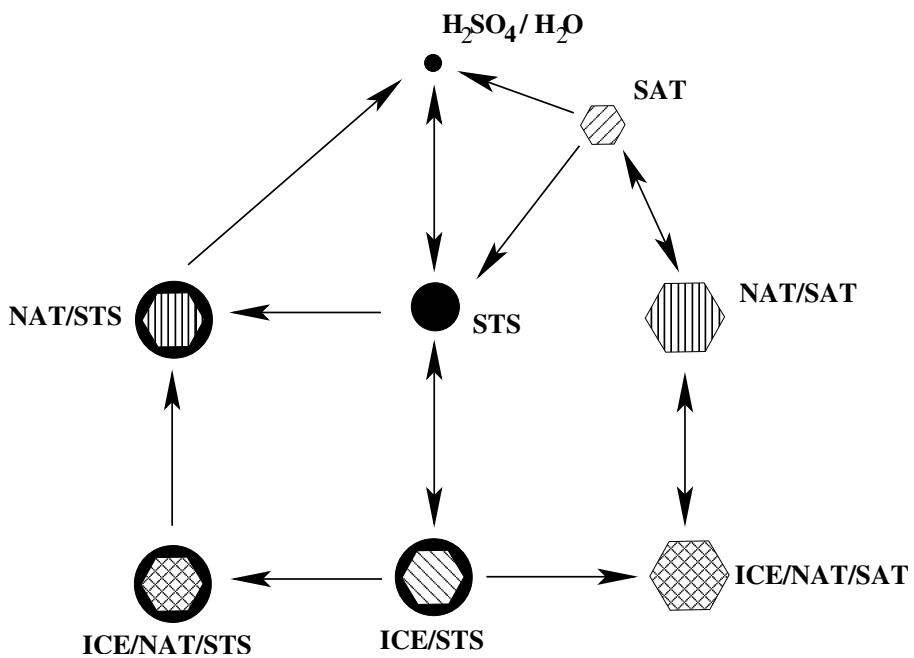

Fig. 3. The STS model of PSC development. Laboratory studies, field observations, and theory suggest that some routes between particle types are bi-directional, while others are only one-way. The NAT/STS and NAT/SAT phases encompass all 'solid' PSC types, including NAT rocks.

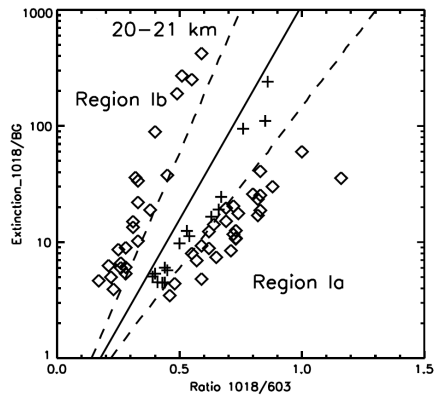

Fig. 4. POAM observations of PSCs during the Arctic winter of 1999/2000 between 20 and 21 km altitude. For each observation the wavelength dependence of the extinction coefficient (shown as the ratio of the 1.018 μm to 0.603 μm extinctions) is plotted against the 1.018 μm extinction coefficient (which is normalised using the background aerosol extinction coefficient). The observations classified as either Type Ia or Ib are shown by the diamonds (in the relevant region); the crosses represent undetermined observations. The solid line represents the division between the criteria for the two different types of cloud, while the dashed lines represent the uncertainty envelope for this division. From Strawa et al. (2002). Copyright 2002 American Geophysical Union. Reproduced by permission of American Geophysical Union.

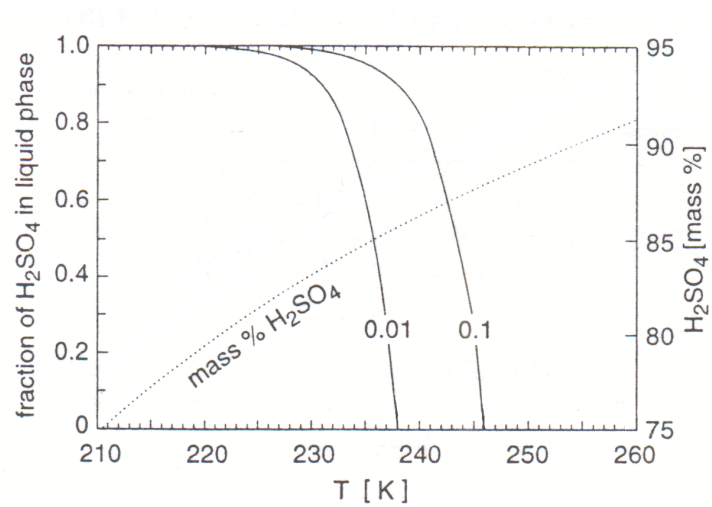

Fig. 5. Phase of sulphuric acid at 10 mbar ($\sim$ 30 km) altitude against temperature, assuming 5 ppmv water vapour. The solid lines indicate the fraction of the total H_2SO_4 (left-hand scale) present in the condensed phase for 0.01 and 0.1 ppbv total H_2SO_4. The dotted line indicates shows the mass fraction of H_2SO_4 (right-hand scale) in binary H_2SO_4/H_2O droplets in equilibrium with the specified water vapour mixing ratio and temperature. Adapted from Carslaw et al. (1997).

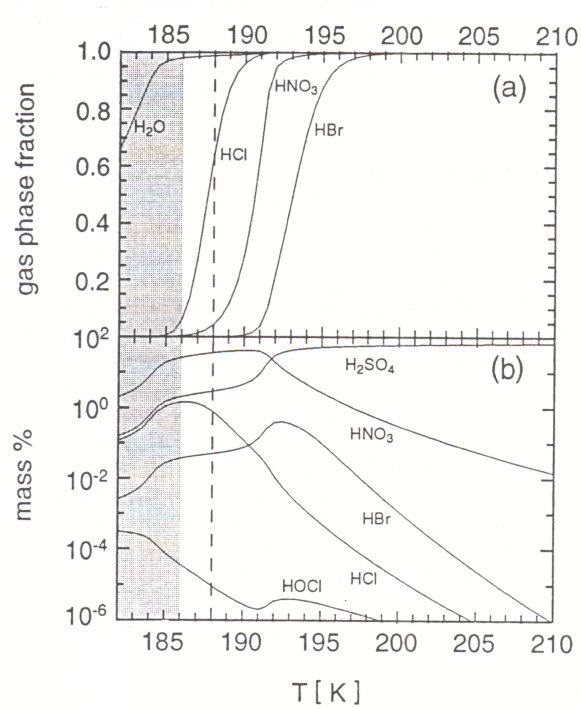

Fig. 6. Partitioning of stratospheric gases into aerosol droplets: (a) fraction of each species in gas phase, and (b) mass fraction of each species in the condensed phase. The vertical dashed line at 188 K indicates the ice frost point. The aerosols are unlikely to remain purely liquid more than a couple of degrees below the frost point, so the system properties within the shaded region are hypothetical. The simulated conditions are 50 mbar altitude, with total amounts of each species a follows: H_2O, 5 ppmv; H_2SO_4, 0.5 ppbv; HNO_3, 10 ppbv; HCl, 1 ppbv; HBr, 0.01 ppbv; HOCl, 0.01 ppbv. The model of Carslaw et al. (1995) was used for these calculations, except for HOCl, which Carslaw et al. (1997) calculated using an adapted version of the H_2SO_4-solution model of Huthwelker et al. (1995). From Carslaw et al. (1997). Copyright 1997 American Geophysical Union. Reproduced by permission of American Geophysical Union.

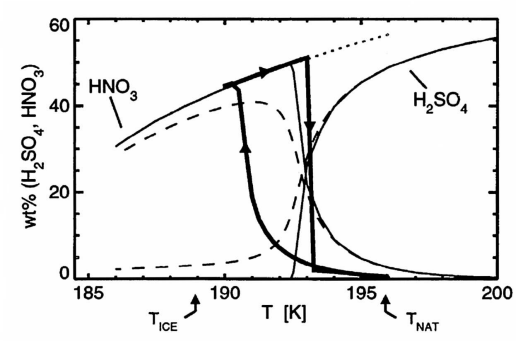

Fig. 7. HNO_3 and H_2SO_4 mass fractions in STS droplets. The total mixing ratios for H_2O and HNO_3 are 5 ppmv and 10 ppbv respectively. The dashed lines represent the changes in particle composition during slow adiabatic cooling of the aerosol. The line solid lines show the changes in particle composition during slow adiabatic cooling without gas-phase depletion, while the dotted line indicates the continuation of the HNO_3/H_2O binary curve to high temperatures. The droplet ensemble is subjected to adiabatic cooling from 196 to 190 K at a rate of $6\,\mathrm{K\,hr^{-1}}$, followed by adiabatic warming back to 196 K at the same rate. The thick line indicates the evolution of the HNO_3 mass fraction of a droplet, with radii $\sim$0.007 and $\sim$0.1 μm at temperatures 196 and 190 K respectively, during this event. From Meilinger et al. (1995). Copyright 1995 American Geophysical Union. Reproduced by permission of American Geophysical Union.

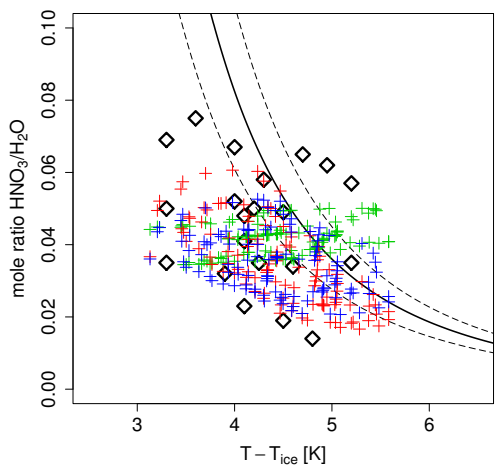

Fig. 8. $HNO_3 : H_2O$ mole ratios in observed STS droplets, plotted as a function of temperature relative to the frost-point T_{ice}. Measurements made by mass spectrometer (diamonds), from Schreiner et al. (1999). Equilibrium mole fractions, calculated after Carslaw et al. (1995), using 5.5 ppmv H_2O, 0.4 ppbv H_2SO_4 and 10 ppbv HNO_3 (solid line). Equilibrium mole fractions for 8 and 12 ppbv HNO_3 are shown as dashed lines. The crosses show the results from a condensed-mass advection model (Lowe, 2003), sampled at fixed radii of 0.09 μm (red), 0.2 μm (blue), and 1.0 μm (green), in a simulation including high frequency temperature fluctuations between 20 and 90 K hr^{-1}. After Voigt et al. (2000b).

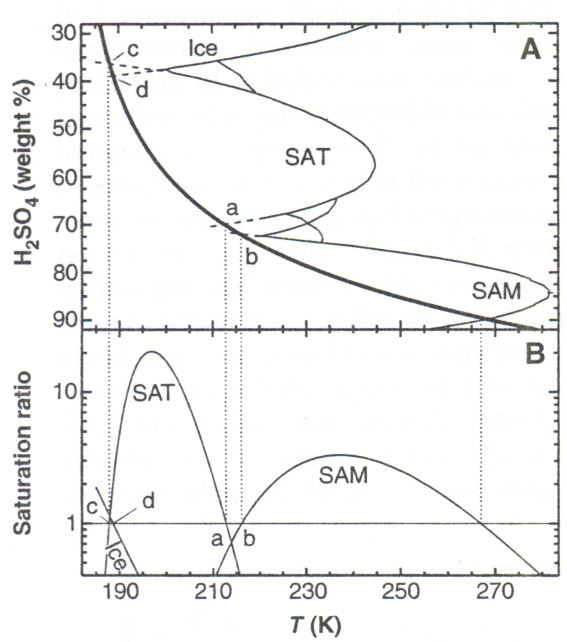

Fig. 9. Comparison of the stability of stratospheric H_2SO_4/H_2O droplets with the different H_2SO_4 solids. The droplets are in equilibrium with a water mixing ratio of 5 ppmv at a 50 mbar altitude. (A) Concentration of droplets (thick solid line) superimposed on the H_2SO_4-H_2O phase diagram. The melting points of the different solid phases (thin solid lines) are taken from Gable et al. (1950). The major solid phases are water ice (H_2O), SAT ($H_2SO_4 \cdot 4H_2O$) and SAM ($H_2SO_4 \cdot H_2O$). The melting points of other minor solid phases ($H_2SO_4 \cdot 6.5H_2O$, $\cdot 3H_2O$, and $\cdot 2H_2O$) are also shown. (B) H_2O saturation ratio with respect to ice, SAT, and SAM. Point d is the ice frost point. From Koop and Carslaw (1996). Reprinted with permission from AAAS.

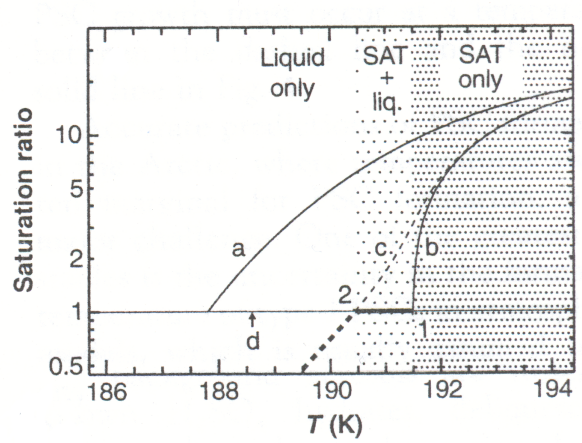

Fig. 10. Saturation ratio of liquid stratospheric aerosols with the same composition as SAT. Line a: pure H_2SO_4/H_2O droplets (as in Fig. 9). Line b: ternary $HNO_3/H_2SO_4/H_2O$ droplets at 50 mbar altitude in equilibrium with 5 ppmv H_2O and a fixed HNO_3 gas phase of 10 ppbv. Line c: same as line b, except with a constant total HNO_3 amount of 10 ppbv, allowing for the partitioning of HNO_3 into the droplets. In the densely shaded region the SAT particles are stable, and therefore remain "dry". Point 1 is the deliquescence temperature of SAT. Between points 1 and 2 (light shading) a STS film coexists with SAT. At point 2 SAT is completely dissolved; below this temperature only purely liquid droplets exist (thick dashed line). Point d is the ice frost point. All solution ratios calculated using the model of Carslaw et al. (1995). From Koop and Carslaw (1996). Reprinted with permission from AAAS.

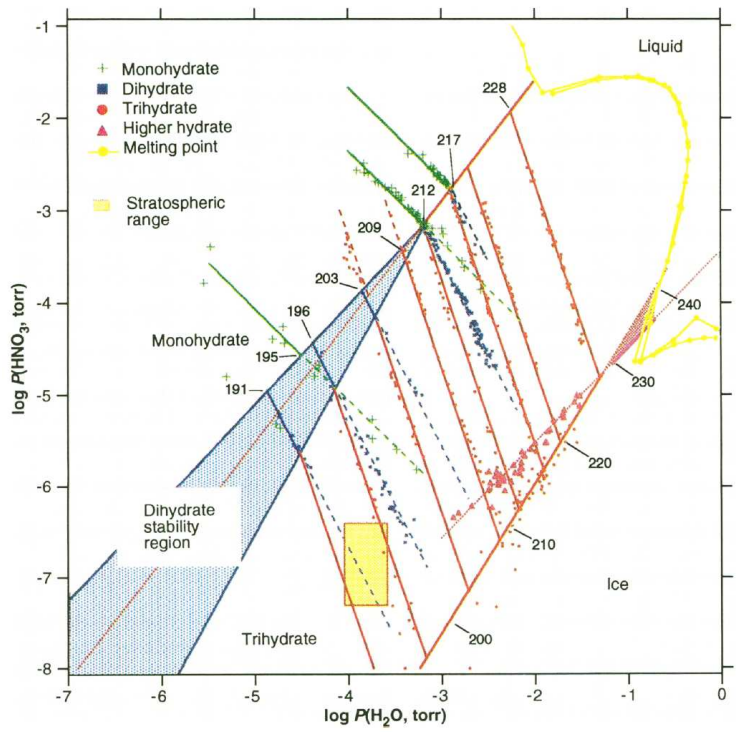

Fig. 11. Nitric acid-water phase diagram (HNO_3 vapour pressure vs. H_2O vapour pressure), with data for the different phases coded by colour and symbol as shown in the key. Lines with positive slopes delineate phase boundaries between (from the lower righthand corner) ice, $HNO_3 \cdot 3H_2O$, $HNO_3 \cdot 2H_2O$, and $HNO_3 \cdot H_2O$ for stable (solid lines) and metastable (dotted lines) phases. The colour-coded lines with negative slopes indicate fits to composition data at the specified temperature. Again solid and dashed lines denote stable and metastable phases, respectively. The blue shaded area indicates the region of stability for $HNO_3 \cdot 2H_2O$. The yellow shaded area indicates the typical range of stratospheric conditions. From Worsnop et al. (1993). Reprinted with permission from AAAS.

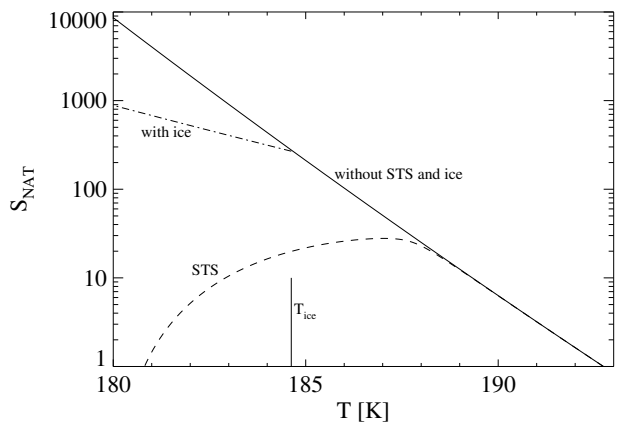

Fig. 12. NAT saturation ratios as a function of temperature, with 5 ppm H_2O, 8 ppb HNO_3, and 0.2 ppb H_2SO_4. The solid line indicates the saturation ratio without STS and ice. The dashed line indicates the saturation ratio for a gas-phase in equilibrium with STS. The dashed and dotted line indicates the saturation ratio for a gas-phase in equilibrium with ice. From Luo et al. (2003). Copyright 2003 American Geophysical Union. Reproduced by permission of American Geophysical Union.

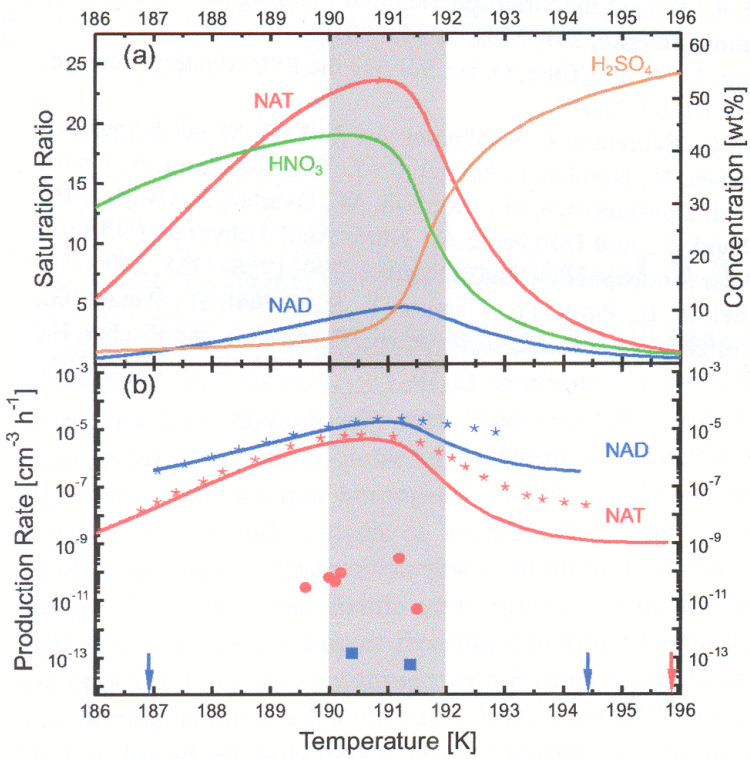

Fig. 13. (a) The compositions (green and orange lines) and the saturation ratios (red and blue lines) of STS aerosols as a function of temperature at 50 mbar with 5 ppmv H_2O, 10 ppbv HNO_3 and 0.5 ppbv H_2SO_4 (Carslaw et al., 1994). The shaded region indicates the temperature range where the saturation ratios over NAD and NAT are at their maximum. (b) Hourly production rates of NAD and NAT particles (blue and red, respectively) per cm^3 of air derived from nucleation rate coefficients for the conditions shown in panel (a). The solid lines indicate the production rates in STS droplets calculated using the formulation of Tabazadeh et al. (2001). The squares and circles indicate the production rates derived from the experimental data of Knopf et al. (2002). The stars show values for similar conditions taken from Fig. 1 of Tabazadeh et al. (2001) (produced using a constant total aerosol volume, unlike the other production values which are calculated using temperature dependent aerosol volumes). The arrows indicate the temperatures at which the saturation ratios of NAD (blue) and NAT (red) equal one. From Knopf et al. (2002). By permission of Copernicus Publications on behalf of the European Geosciences Union.

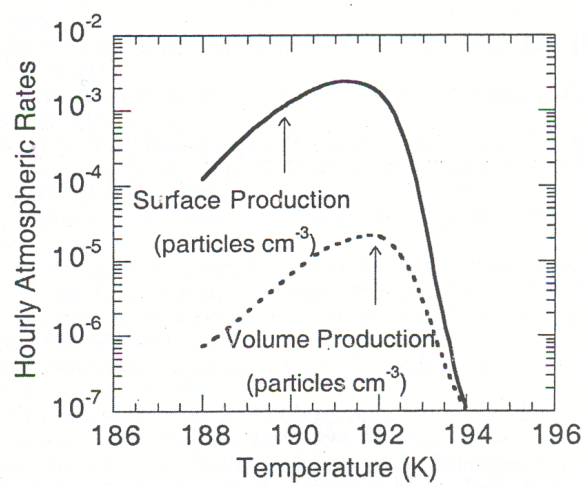

Fig. 14. Comparison of the volume and surface production rates of NAD particles as a function of temperature at 60 mbar with 5 ppmv H_2O, 12 ppbv HNO_3 and 0.5 ppbv H_2SO_4. Reprinted in part, with permission, from Tabazadeh et al. (2002a) Copyright 2002 American Chemical Society.

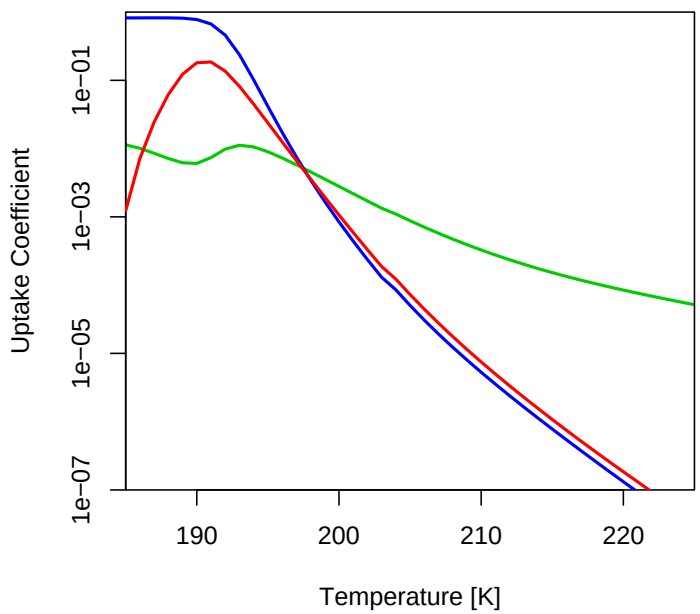

Fig. 15. Reactive uptake coefficients as a function of temperature for heterogeneous reactions occuring in liquid sulphuric acid aerosols. Reaction $ClONO_2 + H_2O$ is represented by the green line, $ClONO_2 + HCl$ by the blue line and $HOCl + HCl$ by the red line. The uptake coefficients are calculated using the parameterisation of Shi et al. (2001), which takes into account the couplings of these reactions.

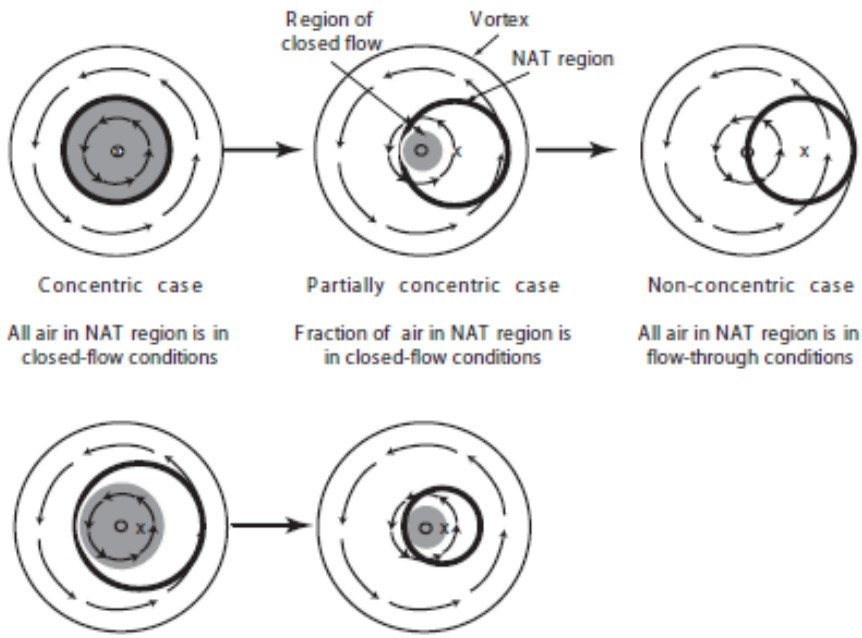

Fig. 16. Schematic of how the concentricity of the vortex and the area of air with temperatures below T_{NAT} (labelled "NAT region"), and the area of the "NAT region", control the denitrification rate. The "closed-flow" region is shaded. The upper row of diagrams illustrate the effect of shifting the NAT region away from the centre of the vortex; the lower row the effect of reducing the size of the "NAT region." From Mann et al. (2003). By permission of Copernicus Publications on behalf of the European Geosciences Union.

PSC Type	Backscatter ratio	α	Depolarisation, %
1a	0.2–0.5	0.4	30–50
1b	2–7	2–3	0.5–2.5
2	> 10	< 0.8	> 10

Table 1

Typical PSC lidar properties when measured using a wavelength of 0.603 μm (Browell et al., 1990).